https://doi.org/10.5194/gmd-2023-235
Preprint. Discussion started: 18 December 2023

Geoscientific Model Development Discussions
Open Access
EGU

RCEMIP-II: Mock-Walker Simulations as Phase II of the Radiative-Convective Equilibrium Model Intercomparison Project

Allison A. Wing[1], Levi G. Silvers[2], and Kevin A. Reed[2]

[1]Department of Earth, Ocean, and Atmospheric Science, Florida State University
[2]School of Marine and Atmospheric Sciences, Stony Brook University

Correspondence: Allison A. Wing (awing@fsu.edu)

Abstract. The Radiative-Convective Equilibrium (RCE) Model Intercomparison Project (RCEMIP) leveraged the simplicity of RCE to focus attention on moist convective processes and their interactions with radiation and circulation across a wide range of model types including cloud-resolving models (CRMs), general circulation models (GCMs), single column models, global cloud-resolving models, and large eddy simulations. While several robust results emerged across the spectrum of models that participated in the first phase of RCEMIP (RCEMIP-I), two points that stand out are (1) the strikingly large diversity in simulated climate states and (2) the strong imprint of convective self-aggregation on the climate state. However, the lack of consensus in the structure of self-aggregation and its response to warming is a barrier to understanding. Gaining a deeper understanding of convective aggregation and tropical climate will require reducing the degrees of freedom with which convection can vary. Therefore, we propose a Phase II of RCEMIP (RCEMIP-II) that utilizes a prescribed sinusoidal sea surface temperature (SST) pattern to provide a constraint on the structure of convection and move one critical step up the model hierarchy. This so-called "mock-Walker" configuration generates features that resemble observed tropical circulations. The specification of the mock-Walker protocol for RCEMIP-II is described, along with example results from one CRM and one GCM. RCEMIP-II will consist of five simulations covering the three mean SST's as in RCEMIP-I but imposing three different SST gradients. We also test the sensitivity to the imposed SST gradient and the domain size. Under weak SST gradients, unforced self-aggregation emerges across the entire domain but as the SST gradient increases, the convective region narrows and is confined to the warmest SSTs. At warmer mean SSTs and stronger SST gradients, low-frequency variability of the convective aggregation emerges, suggesting that simulations of at least 200 days may be needed to achieve robust equilibrium statistics in this configuration. Simulations with different domain sizes generally have similar mean statistics and convective structures, depending on the value of the SST gradient. The prescribed SST boundary condition is the only difference in the set-up between RCEMIP-II and RCEMIP-I, which enables comparison between the two. However, we also welcome participation in RCEMIP-II from models that did not participate in RCEMIP-I.

1 Introduction

On Earth, the tropics play an important role in climate through coupled interactions of clouds, circulation, and radiative fluxes. As such, tropical regions influence the global energy balance and tropical variability has far-reaching global effects on weather

https://doi.org/10.5194/gmd-2023-235
Preprint. Discussion started: 18 December 2023

Geoscientific Model Development Discussions
Open Access
EGU

patterns and extremes. Thus, understanding the underlying mechanisms that connect climate, clouds and circulation remains paramount in climate science, particularly in the context of global warming (Bony et al., 2015). Operational models, such a global forecast models and general circulation models, have evolved over recent decades to advance our understanding and simulation of the tropics, but biases and uncertainty in climate projections remain. The links between tropical circulation and clouds on a wide range of space and time scales are complicated by a host of scale interactions that limit our ability to understand and effectively use comprehensive Earth system models (Held, 2005).

Given the complexities of these interactions, theory and idealized models of the tropical atmosphere are important tools for advancing understanding. Idealization allows for experiments that target specific features of interest, while retaining the fundamental properties of the tropical climate. Furthermore, the simplicity and flexibility of idealized models provides an opportunity for developing new understanding. One line of idealized modeling has focused on radiative-convective equilibrium (RCE), which approximates the tropical atmosphere as a statistical balance between radiative cooling and convective heating. RCE represents the simplest approximation of not only the tropics, but global climate more broadly. There has been a long history exploring RCE in idealized models for advancing understanding of the tropics (e.g., Manabe and Strickler, 1964; Held et al., 1993; Tompkins and Craig, 1998; Satoh et al., 2016; Held et al., 2007; Popke et al., 2013).

The RCE Model Intercomparison Project (RCEMIP; Wing et al., 2018) was a coordinated international effort to standardize the boundary conditions and forcing assumptions of RCE simulations to allow for the intercomparison across various atmospheric model types. RCEMIP included cloud-resolving models (CRMs), large eddy simulation models (LES), global cloud-resolving models (GCRMs) and general circulation models (GCMs). The initial phase of RCEMIP (hereafter RCEMIP-I) focused on changes in clouds and convective activity with surface warming, as well as associated cloud feedbacks, the implications for climate sensitivity, and the role of aggregation in tropical climate. Results of RCEMIP-I have revealed robust behaviors across the model hierarchy, such as the response of deep convective clouds to warming (Wing et al., 2020a; Stauffer and Wing, 2022, 2023a, b), the existence of self-aggregation and its influence on the mean state (Wing et al., 2020a), the importance of cloud-radiative feedbacks in driving self-aggregation (Pope et al., 2023), the response of the large-scale circulation to warming (Silvers et al., 2023), and the modulation of cloud feedbacks and climate sensitivity by self-aggregation (Becker and Wing, 2020; Stauffer and Wing, 2023b). However, the intercomparison also revealed diverse results, including substantial disagreement in the representation of mean profiles of temperature, humidity, and cloudiness, a wide range of static stability and climate sensitivities, a large variation in the degree of convective aggregation, and no consensus in the response of aggregation to warming (Wing et al., 2020a; Becker and Wing, 2020; Wing and Singh, 2023; Silvers et al., 2023).

RCEMIP-I prescribed homogeneous boundary conditions, including sea surface temperatures (SST) and forcings (insolation). The simplification of the boundary conditions demonstrates how sensitive the simulation of convection and its complex interactions with radiation and circulation are to model design. The divergent behavior in RCEMIP-I reveals the sensitivities to representations of convection, microphysics, turbulence, and dynamical cores; sensitivities that may have been masked in other intercomparisons by dynamical constraints. To build on this work we proposal a second phase of RCEMIP (hereafter RCEMIP-II) in which standardized heterogeneities in the SST are now prescribed to explore robust behaviors in the tropical system when more realistic, but still idealized, circulations are included in RCE.

https://doi.org/10.5194/gmd-2023-235
Preprint. Discussion started: 18 December 2023


Geoscientific Model Development Discussions

A "mock-Walker" circulation (Raymond, 1994) confines deep convection to regions of low-level convergence and large-scale ascent, determined by the SST pattern (Lindzen and Nigam, 1987; Bretherton and Sobel, 2002; Back and Bretherton, 2009). The general features resemble observed tropical circulations (Grabowski et al., 2000), reflecting an interplay of convection, radiation, humidity, and large-scale circulation that is fundamental to tropical deep convective regions (Bretherton et al., 2006). While the SST pattern fixes the location of the circulation and constrains its strength, interactions between convection, surface gustiness, water vapor, and radiation modify the large-scale flow and the strength and spatial extent of convection (Tompkins, 2001; Liu and Moncrieff, 2008; Wofsy and Kuang, 2012; Silvers and Robinson, 2021). Cloud radiative feedbacks narrow the convective region in a manner reminiscent of self-aggregation (Grabowski et al., 2000; Bretherton and Sobel, 2002; Liu and Moncrieff, 2008), similar to the zonal contraction of convection in spherical simulations with zonally uniform, meridionally varying SST (Müller and Hohenegger, 2020).

The prescribed SST gradient in the RCEMIP-II mock-Walker simulations will drive a large-scale circulation that provides a constraint on the structure of convection, compared to RCE in which there are no external constraints on the location or spatial pattern of convection. The "forced" aggregation in RCEMIP-II is hypothesized to reduce the intermodel spread in the simulated climate state, while still allowing for "un-forced" self-aggregation intrinsic to the model to emerge via radiative-convective feedbacks (e.g., Grabowski et al., 2000; Bretherton and Sobel, 2002; Liu and Moncrieff, 2008; Müller and Hohenegger, 2020). By varying the strength of the SST gradient with warming, the impact of aggregation on climate sensitivity will be able to be attributed to the forced vs. unforced aggregation. An additional motivation for the simulations described below is that mock-Walker simulations are a valuable component of the model hierarchy for tropical dynamics (Jeevanjee et al., 2017) and can still be performed by both CRMs and GCM-like models in limited-area planar domains and GCMs on the global sphere. By changing just one parameter compared to the RCEMIP-I simulations (the analytic SST boundary condition) the proposed RCEMIP-II simulations represent a single, clean move up the model hierarchy of model complexity that is closer to the observed tropics than RCE.

This paper is organized as follows. Section 2 provides an overview of the scientific objectives for RCEMIP-II. The experimental design, which builds on RCEMIP-I to add an SST pattern to enable an intercomparison of idealized tropical circulations across the model hierarchy, is provided in Section 3. Section 4 presents sample results for RCEMIP-II to demonstrate the setup and Section 5 provides some next steps and brief discussion.

2 Science Objectives

Our vision for RCEMIP was always that the initial simulations (Wing et al., 2018) would serve as a starting point, but deep understanding would require performing additional simulations to address issues such as the robustness of the results to experimental design, the sensitivity to model physics and dynamics, and the impact of other factors such as ocean-atmosphere interactions or rotation. In considering the RCEMIP-I results, two points that stand out are (1) the strikingly large the spread in simulated RCE states is; and (2) the strong an imprint of convective self-aggregation on the climate state (Wing et al., 2020a). However, the wide range in the degree of self-aggregation and the lack of consensus in its temperature dependence is a barrier

https://doi.org/10.5194/gmd-2023-235
Preprint. Discussion started: 18 December 2023


Geoscientific Model Development Discussions

to understanding. Given these two points, RCEMIP-II includes an additional suite of simulations with a constraint on convection and circulation that should narrow the intermodel spread. Therefore, RCEMIP-II consists of a set of "mock-Walker" simulations with a prescribed sinusoidal SST pattern. RCEMIP was designed to focus on three scientific themes:

1. The robustness of the simulated mean state across the spectrum of models
2. The response of convective clouds to warming and climate sensitivity
3. The dependence of convective self-aggregation on temperature.

The mock-Walker simulations in RCEMIP-II will emphasize the coupling of clouds and circulations as a framework within which these three themes can be further explored to build on the successes of RCEMIP-I. RCEMIP-II will facilitate deeper understanding of cloud-circulation coupling and convective aggregation and its role in climate - including the hydrological cycle, cloud feedbacks, and climate sensitivity - by providing a constraint that is expected to reduce the diversity of simulated climates and provide a clearer tie to observations, while still allowing for the rich interactions between convection, clouds, and circulations.

3 Experimental Design

The experimental design of the RCEMIP-II simulations follows the philosophy set out by RCEMIP-I (Wing et al., 2018); that is, a small set of experiments that are designed to maximize the utility of the simulations in answering the above questions, while minimizing the effort required of modeling groups. **To facilitate comparison with the RCEMIP-I simulations, an identical configuration is used to that described by Wing et al. (2018) *except* for the analytic SST boundary condition.** Participation in RCEMIP-I, while beneficial for comparison, is **NOT** required to participate in RCEMIP-II.

The experimental design for the RCEMIP-II mock-Walker simulations is motivated by model configurations in recent studies of tropical convection and circulation (e.g., Silvers and Robinson, 2021; Lutsko and Cronin, 2018, 2022). Since the simulations are non-rotating and the Cartesian CRM domain is doubly periodic, note that a mock-Walker circulation along the long (x) dimension of the CRM domain is consistent with a meridional circulation forced by a zonally uniform meridionally varying SST in a spherical global model, which has also previously been used to study convective aggregation (e.g., Müller and Hohenegger, 2020). The periodic boundary conditions in the CRM domain means that the SST pattern in effect infinitely repeats in each direction. The meridionally varying SST chosen for the global model is the closest match to this, and also avoids any irregularities that could arise from an SST pattern that decreases in width as the poles are approached, as would be the case for a zonally varying SST.

3.1 Basic model setup

A non-rotating aquaplanet model configuration is to be used (i.e., the Coriolis parameter, f, or Earth's angular velocity, Ω, are set to zero), with no sea ice and no land. Recommended geophysical constants and parameters are provided in Table 1 of Wing et al. (2018), following the convention of the Aqua-Planet Experiment (APE; http://climate.ncas.ac.uk/ape/design.html).

https://doi.org/10.5194/gmd-2023-235
Preprint. Discussion started: 18 December 2023


Geoscientific Model Development Discussions

Models which participated in RCEMIP-I should ideally use the same model version and configuration as RCEMIP-I for their RCEMIP-II mock-Walker simulations, to ensure that the SST boundary condition is the only thing that is different. If this is not possible due to model development in the intervening years, the `RCE_large300` simulation from RCEMIP-I should be repeated with the new version of the model, to represent a reference point.

The RCEMIP-II simulations are to be initialized by the same sounding that was used to initialize a model's RCEMIP-I `RCE_large` simulation at the corresponding mean SST. That is, they should be initialized by a horizontally averaged equilibrium sounding from the corresponding `RCE_small` simulation.

We welcome participation in RCEMIP-II from models that did not participate in RCEMIP-I. Such models should at minimum complete the `RCE_small` simulations described in Wing et al. (2018) to derive a sounding from which to initialize their RCEMIP-II simulations. We encourage but do not require that they complete the RCEMIP-I `RCE_large` simulations, to serve as a reference.

3.2 Domain configuration

The domain configuration follows the `RCE_large` set-up described in Wing et al. (2018), for CRMs, GCMs, or GCRMs, which is reviewed here. SCM models are not eligible to participate in RCEMIP-II and it is likely prohibitively computationally expensive for models at LES resolutions to perform simulations on the RCEMIP-II domain.

3.2.1 CRMs

CRMs (models with explicit convection run on a limited-area planar domain) are to employ a three-dimensional domain with doubly periodic lateral boundary conditions. A horizontal grid spacing of 3 km is to be used with an elongated channel geometry of $\sim$6000 km in the long (x) direction and $\sim$400 km in the short (y) direction. The domain should be as close to 6000 km long as possible given the numerical limitations of a given model. The vertical grid is to be at least 74 vertical levels, a model top no lower than 33 km, and a sponge layer in the top model layers to damp gravity waves. Table 3 in Wing et al. (2018) provides the recommended vertical grid. The simulations are to be performed for at least 200 days.

3.2.2 GCMs

GCMs (models with parameterized convection run on the global sphere) should employ whichever dynamical core and grid are standard for each model and the horizontal resolution, vertical coordinate, and grid of their CMIP6 configuration. We have chosen not to constrain the GCMs to a common horizontal and vertical grid because the physical parameterizations are sensitive to particular configurations. The simulations are to be performed for at least 1000 days.

3.2.3 GCRMs

GCRMs (models with explicit convection run on a sphere) should ideally be run with the same grid spacing as CRMs (3 km) and the same domain size as GCMs (the real Earth radius, R_E). However, a reduced Earth radius may be used to reduce the

https://doi.org/10.5194/gmd-2023-235
Preprint. Discussion started: 18 December 2023

Geoscientific Model Development Discussions

computational expense. A radius of $R_E/3.336$ will yield the correct wavelength of the SST pattern (see below). The simulations are to be performed for at least 200 days.

3.3 Surface boundary condition

Surface enthalpy fluxes are to be calculated interactively from the resolved surface wind speed and air-sea enthalpy disequilibrium. If allowed by a model's surface layer formulation, a minimum wind speed of 1 ms^{-1} should be enforced. The lower boundary represents the thermodynamic state of a sea surface with that is fixed in time but varies spatially according to a prescribed sinusoidal temperature pattern. We desire to keep the mean SST and the SST gradient (change in SST per unit distance) as consistent as possible between the Cartesian CRM and spherical GCM configurations.

3.3.1 CRMs

For CRMs on the cartesian channel domain described above,

$$SST(x) = \langle SST \rangle - \frac{\Delta SST}{2} cos\left(\frac{2\pi x}{L_x}\right), \tag{1}$$

where $\langle SST \rangle$ is the mean SST, ΔSST is the difference between the maximum SST and the minimum SST, x is the horizontal position along the long axis, and L_x is the domain length. This sets the wavelength of the SST pattern, λ, equal to L_x and places the maximum SST at $L_x/2$, to maintain periodicity at the lateral boundaries. Because the CRMs participating in RCEMIP use slightly different domain lengths, due to code numerics optimization and limitations, this means that the wavelength, and thus the SST gradient (dSST/dx), will vary slightly across models. Over the range of L_x in the RCEMIP-I simulations, the resulting SST gradients differ from that with L_x = 6000 km by less than 3% (except for one model that used L_x = 6480 km, which has an SST gradient that is 7.4% smaller than that with L_x = 6000 km. While not ideal, this situation is more desirable than the alternative, which is to set λ = 6000 km regardless of the domain length. This alternative would lead to slightly different $\langle SST \rangle$ across the models, a discontinuous SST distribution at the boundaries (since $\lambda \neq L_x$), and, most critically, the projection of the prescribed SST forcing onto all scales. The first two are minor issues, but while the vast majority of the power would be in the desired domain-scale wave, $\lambda \neq L_x$ introduces substantial noise at higher wavenumbers (contributing to the majority of the variance of $dSST^2/dx^2$). Therefore, in order to avoid non-physical artifacts of the set-up, we elect to use Equation 1 to define the SST in the CRMs, but acknowledge that the SST gradients may differ slightly across models if their $L_x \neq 6000$ km.

3.3.2 GCMs

For GCMs on a sphere using the observed radius of Earth,

$$SST(\phi) = \langle SST \rangle + \frac{\Delta SST}{2} cos\left(\frac{360° \phi}{\lambda}\right), \tag{2}$$

where $\langle SST \rangle$ is the mean SST, ΔSST is the difference between the maximum SST and the minimum SST, ϕ is latitude in degrees, and $\lambda = 54°$ yields a wavelength of 6004.53 km (for the wavelength centered on the equator), to approximately match

https://doi.org/10.5194/gmd-2023-235
Preprint. Discussion started: 18 December 2023

Geoscientific Model Development Discussions

Table 1. RCEMIP-II Experiments

Experiment Name	$\langle SST \rangle$	ΔSST
`MW_295dT1p25`	295 K	1.25 K
`MW_300dT0p625`	300 K	0.625 K
`MW_300dT1p25`	300 K	1.25 K
`MW_300dT2p5`	300 K	2.5 K
`MW_305dT1p25`	305 K	1.25 K

the CRM configuration. Note that since these simulations are non-rotating there is no dynamical difference between a wave in latitude and a wave in longitude. The wave in latitude proposed here maintains a consistent distance between each peak that is comparable to that in the CRM domain.

3.3.3 GCRMs

For GCRMs on a sphere with reduced Earth radius of R_E/n, where R_E is the observed radius of Earth,

$$SST(\phi) = \langle SST \rangle + \frac{\Delta SST}{2} cos\left(\frac{360° \phi}{\lambda}\right), \tag{3}$$

where $\langle SST \rangle$ is the mean SST, ΔSST is the difference between the maximum SST and the minimum SST, and ϕ is latitude in degrees. For $n = \pi R_E/6000km$, which yields a radius of $R_E/n \approx R_E/3.336$, $\lambda = 180°$ corresponds to distance of 6000 km, to match the CRM configuration. If a smaller Earth radius of $R_E/4$ is used, as was used by some GCRMs in RCEMIP-I, $\lambda = 180°$ corresponds to a distance of approximately 5000 km. Smaller Earth radii than this are not recommended.

3.4 Radiative processes

The shortwave and longwave radiative heating rates are to be calculated interactively from the modeled state using a radiative transfer model. Trace gases are to be fixed and spatially uniform, according to Table 2 in Wing et al. (2018). The ozone profile is an analytic approximation of the horizontally uniform equatorial profile derived from the Aqua-Planet Experiment ozone climatology, given by Equation (1) in Wing et al. (2018). Aerosol effects are to be ignored. The incoming solar radiation is to be spatially uniform and constant in time; there is no diurnal nor seasonal cycle and every model grid point should receive the same incident radiation. Following Wing et al. (2018), a reduced solar constant of 551.58 W m^{-2} and a fixed zenith angle of 42.04° should be used.

3.5 Required simulations

The five required RCEMIP-II experiments are listed in Table 1. Figure 1 shows the SST pattern in each experiment. In selecting the suite of ΔSST values, we took inspiration from, but did not attempt to exactly reproduce, observed SST gradients in the

https://doi.org/10.5194/gmd-2023-235
Preprint. Discussion started: 18 December 2023

Geoscientific Model Development Discussions

equatorial Pacific and Atlantic. Based on the 1950-2022 HadISST (Rayner et al., 2023) climatological SSTs, averaged between 5.5°S and 5.5°N, there is a difference between the warmest and coldest SSTs of ∼4 K over a distance of 14,344 km in the Pacific (between longitudes of 140.5° to -90.5°) and ∼2 K over a distance of 6,783 km in the Atlantic (between longitudes of -50.5° to 10.5°). In both basins, the climatological mean SST is ∼300 K. We desire to use an identical domain configuration as in RCEMIP-I, so that the simulations can be compared. This sets λ = 6000 km, to accommodate a full wavelength with the warmest SSTs at the center of the domain, doubly periodic lateral boundary conditions, and the the `RCE_large` CRM domain length of $L_x \sim$ 6000 km. Thus, a difference between the warmest and coldest SSTs of ΔSST = 0.83-0.89 K over 3000 km (half a wavelength) would be comparable to the observed SST gradients.

We considered three different values of $\langle SST \rangle$ (295, 300, and 305 K) and nine different values of ΔSST (0.625, 0.75, 1.0, 1.25, 1.5, 2.0, 2.5, 3.0, 5.0 K). Our central value of $\langle SST \rangle$ = 300 K is consistent with current observed mean SSTs in the equatorial Pacific and Atlantic. For the three values of ΔSST at $\langle SST \rangle$ = 300 K (Table 1, Figure 1), we selected values that resulted in distinctly different weak, moderate, and strong SST gradients, balancing similarity to observations with choices that have distinct spatial structures of convection and circulation. Our control experiment (`MW_300dT1p25`) thus has an SST gradient that is ∼45% stronger than observed. `MW_300dT0p65` and `MW_300dT2p5` consider SST gradients that are half and twice as strong as the control; `MW_300dT0p65` has an SST gradient that is ∼37% weaker than observed while `MW_300dT2p5` has an SST gradient that is ∼190% stronger than observed.

The additional `MW_295dT1p25` and `MW_305dT1p25` simulations, along with `MW_300dT1p25`, will reveal the effect of uniform warming on the large-scale circulation, convective aggregation, and other features of the simulated climate. This set of simulations can be compared to the corresponding `RCE_large` simulations with the same mean SSTs from RCEMIP-I, to evaluate the impact of the SST gradient and forced circulation on both the model mean state and response to warming. One slight caveat is that, assuming the weak temperature gradient condition, the domain mean free tropospheric temperature in the RCEMIP-II simulations will be set not by the the mean SST, but by the warmest SST (where deep convection is expected to occur). In the RCEMIP-I simulations, the SST is uniform. Thus, there will be a slight difference between the expected mean free tropospheric temperatures in the RCEMIP-II simulations and the RCEMIP-I simulations at the same mean SST.

The set of required RCEMIP-II simulations will also be used to study the response to warming with the SST gradient held constant, decreased, and increased, respectively. Changing ΔSST under mean warming to amplify or dampen the SST pattern will change the strength of the large-scale circulation and the forced component of aggregation, whereas when ΔSST is kept fixed, only changes in unforced aggregation will occur. This will facilitate improved understanding of the modulation of climate and hydrological sensitivity by convective aggregation, by having ΔSST as an external parameter that controls the forced component of aggregation. The pattern of SST warming also influences climate feedbacks. That is, when ΔSST is reduced with mean SST warming, the cold regions warm more than the warm regions (where deep convection is confined), but when ΔSST is enhanced with mean SST warming, the warm regions warm more than the cold regions. Thus we will also be able to assess how different models represent the pattern effect, which has not previously been examined in a model ensemble that includes models with explicit convection.

https://doi.org/10.5194/gmd-2023-235
Preprint. Discussion started: 18 December 2023

Geoscientific Model Development Discussions
Open Access
EGU

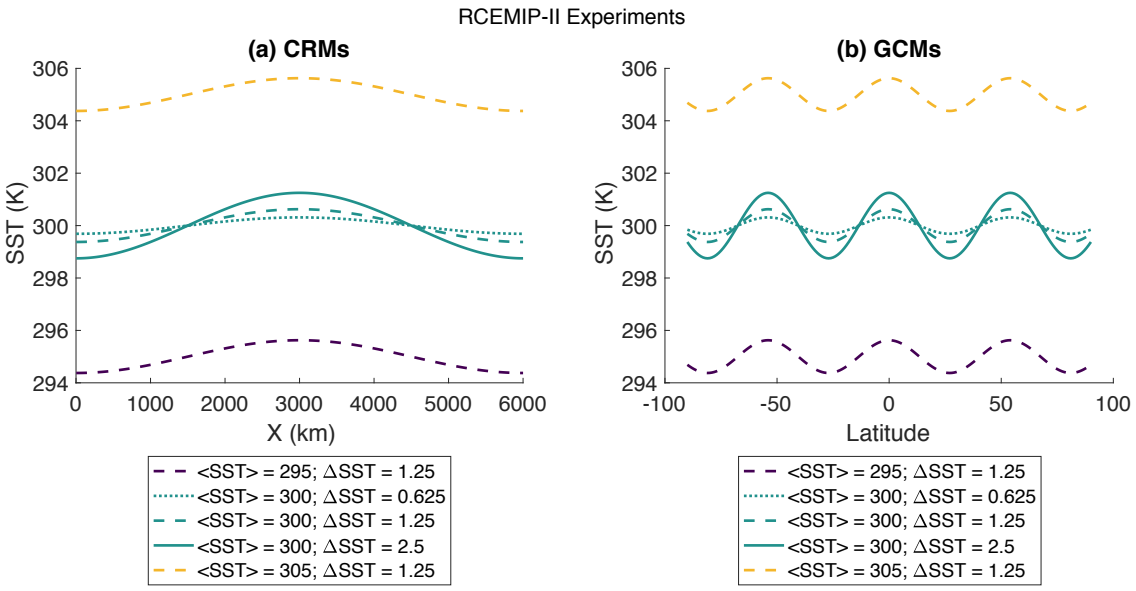

Figure 1. SST pattern for the five required RCEMIP-II experiments, for (a) a CRM with domain length $L_x = \lambda$ = 6000 km; and (b) a GCM with real Earth radius and $\lambda = 54°$.

4 Results

We performed test simulations using the System for Atmospheric Modeling (SAM, a CRM), version 6.11.2 (Khairoutdinov and Emanuel, 2013) and the Community Atmosphere Model (CAM, a GCM), version 6 (Danabasoglu et al., 2020). Similar to the paper describing the RCEMIP-I protocol (Wing et al., 2018), we show here sample results from some of these test simulations with SAM and CAM to motivate our choice of required simulations for the RCEMIP-II protocol and as an example of what those simulations might look like; this is not intended as a comprehensive comparison.

The SAM simulations shown in Figures 2, 7, and 8 use Equation 1 to set the SST pattern as required for RCEMIP-II, with $L_x = \lambda = 6144$ km (L_x = 6000 km is not possible due to numerical and code optimization limitations). The SAM simulations used to test the value of ΔSST in Figures 4 and 6, and used to test the domain size in Figures 9, 10, and 11, were performed before Equation 1 was set and thus instead used $SST(x) = \langle SST \rangle + \frac{\Delta SST}{2} cos\left(\frac{2\pi}{L_x}\left(x + \frac{L_x}{2}\right)\right)$ with λ = 6000 km and L_x = 6144 km. While the details of an individual simulation with λ = 6000 km versus λ = 6144 km vary, the conclusions regarding the dependence on ΔSST and domain size do not qualitatively depend on this difference. Other than the SST boundary condition, the SAM simulations are identical to their configuration for RCEMIP-I.

The CAM simulations shown all use Equation 2 with $\lambda = 54°$, as required by RCEMIP-II. The CAM simulations use the version 6 physics package as in RCEMIP-I (Wing et al., 2020a; Reed et al., 2021) but have been updated to improve some flaws

https://doi.org/10.5194/gmd-2023-235
Preprint. Discussion started: 18 December 2023

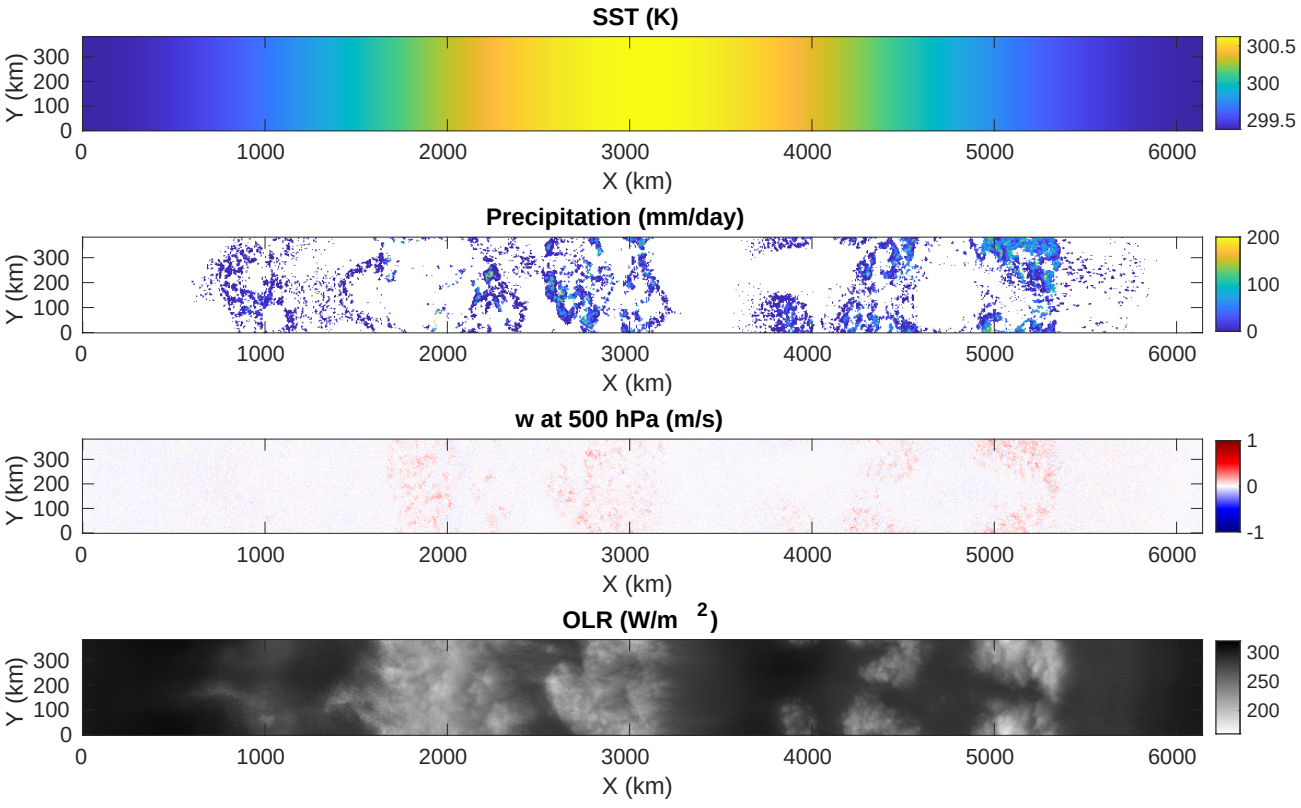

Figure 2. Daily-mean SST (K), precipitation (mm d^{-1}), vertical motion at 500 hPa (m s^{-1}), and outgoing longwave radiation (OLR; W m^{-2}) at day 150 in the `MW_300dT1p25` simulation with SAM.

in the cloud microphysics and ice nucleation (Zhu et al., 2022). Comprehensive climate simulations with the updated version of the Community Earth System Model, version 2 (CESM2) result in a lower equilibrium climate sensitivity, a more realistic Last Glacial Maximum, and a weaker shortwave cloud feedback than the version of CESM2 submitted to CMIP6 (Zhu et al., 2022), from which the version of CAM6 used in RCEMIP-I was drawn (Reed et al., 2021). Therefore, we rerun the RCEMIP-I simulations with this updated version of CAM6 as well for comparison.

4.1 Convective Structure and Evolution

Figures 2 - 3 show the spatial structure in the `MW_300dT1p25` simulation. Deep convection and precipitation are generally absent from the regions of coldest SSTs. In SAM, where there is one peak in SST at the center of the domain, the precipitation and low values of outgoing longwave radiation (OLR) associated with cold cloud tops are located in the region of the warmest

https://doi.org/10.5194/gmd-2023-235
Preprint. Discussion started: 18 December 2023

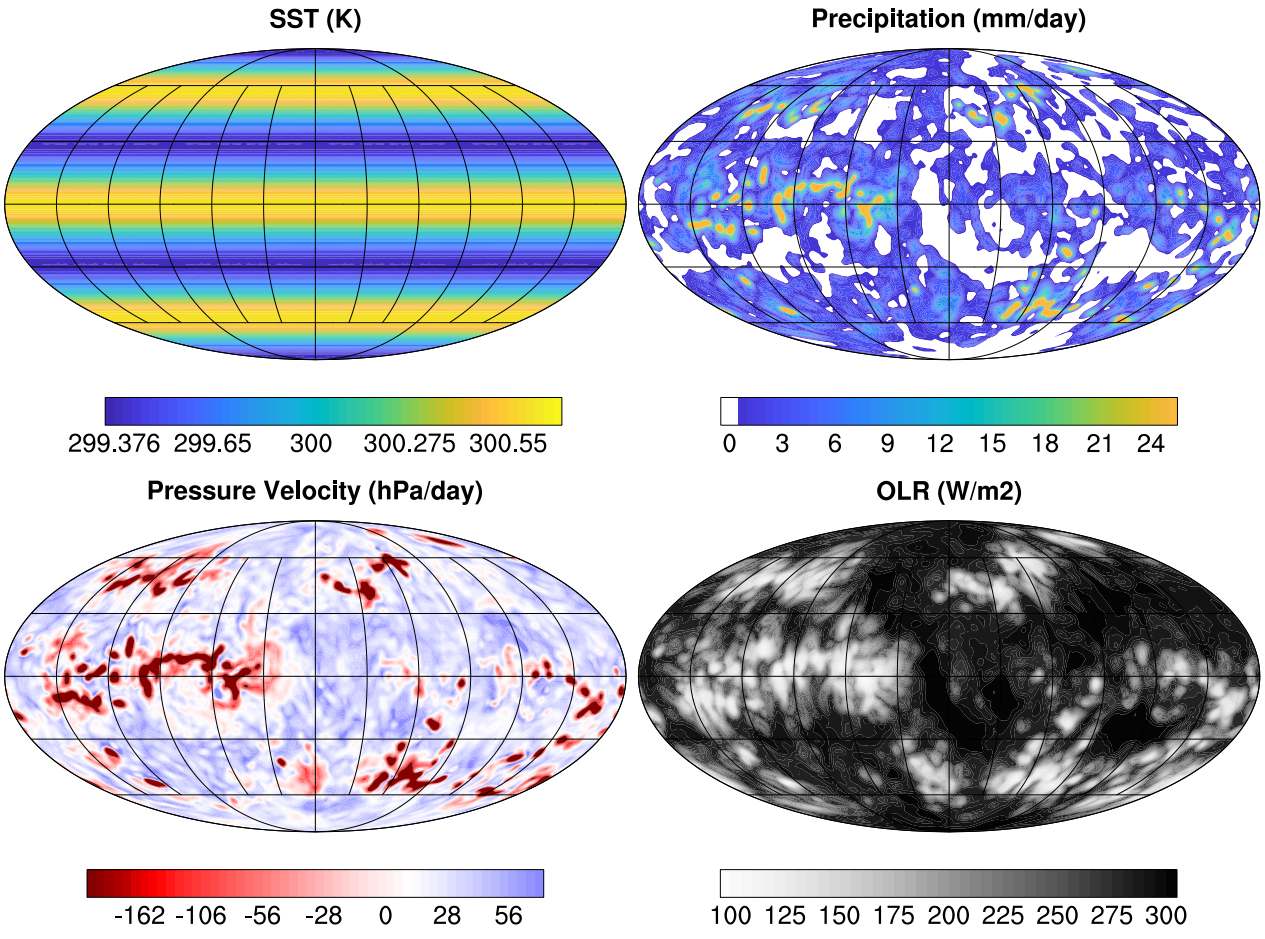

Figure 3. SST (K), precipitation (mm day^{-1}), vertical pressure velocity on the 500 hPa pressure level (hPa d^{-1}), and the outgoing longwave radiation (W m^{-2}), averaged over 1 day in the third year of the `MW_300dT1p25` simulation with CAM.

https://doi.org/10.5194/gmd-2023-235
Preprint. Discussion started: 18 December 2023

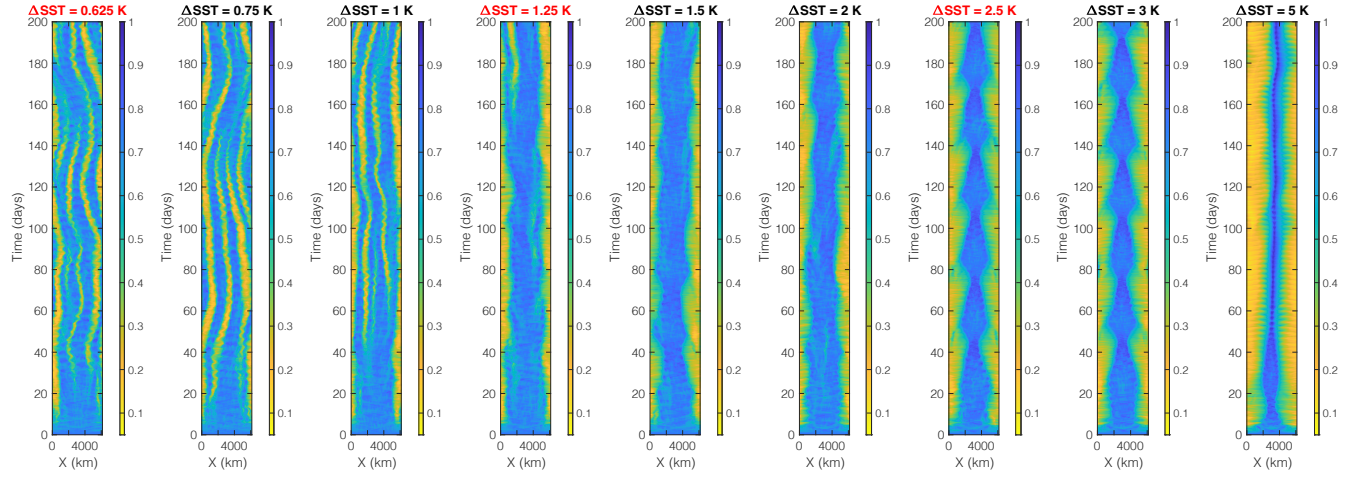

Figure 4. Hovmöller diagrams of y-averaged column relative humidity in the simulations with $\langle SST \rangle$ = 300 and ΔSST = 0.625, 0.75, 1, 1.25, 1.5, 2, 2.5, 3, and 5 K, with SAM. The values of ΔSST that are required for RCEMIP-II are highlighted in red. Note that these SAM simulations, used to test the value of ΔSST, were performed with $SST(x) = \langle SST \rangle + \frac{\Delta SST}{2} cos\left(\frac{2\pi}{L_x}\left(x + \frac{L_x}{2}\right)\right)$ with λ = 6000 km and L_x = 6144 km, rather than Equation 1 and $\lambda = L_x$ as required for RCEMIP-II.

SSTs and their periphery. There are numerous convective systems within the envelope of warm SST. In CAM, an SST pattern with three peaks in latitude is used to match the spatial scale of the SST pattern used by SAM. As a result the CAM results show three latitudinal bands of precipitation. However within these latitudinal bands, there are certain longitudes with more precipitation than others. This varies with time (only a single time is shown in the figure) and is similar to the zonal contraction of convection in the simulations of Müller and Hohenegger (2020).

Figures 4-5 show the temporal evolution of column relative humidity in a set of simulations with $\langle SST \rangle$ = 300 K and different values of ΔSST. Column relative humidity is defined as the ratio of the water vapor path to the saturated water vapor path. Localization of convection associated with the development of dry and moist patches emerges within the first twenty days of the simulations, though it takes more than fifty days for the simulations to reach a statistical equilibrium. The localized dry patches are more spatiotemporally intermittent in CAM (Figure 5) than SAM (Figure 4), especially at the lower values of $\langle SST \rangle$. However, note that Figure 5 depicts the average across a random 4° of longitude, to average over a region roughly consistent with the SAM domain. Other moist and dry patches are found at other longitudes (and latitudes) in the SAM simulation, though Hovmöller diagrams of the zonal mean column relative humidity are qualitatively similar to Figure 5, albeit smoother. While only the first 200 days are plotted, the CAM simulation is run for over 1000 days. The structure of column relative humidity is remarkably consistent to what is shown in Figure 5 over the full simulation. The only exception is that in the `MW_300dT5`, the moist band near the equator breaks down around day 350, before re-emerging by day 450 (not shown). This could indicate the moist band moving to a different longitude, or it could suggest a temporary reorganization

https://doi.org/10.5194/gmd-2023-235
Preprint. Discussion started: 18 December 2023

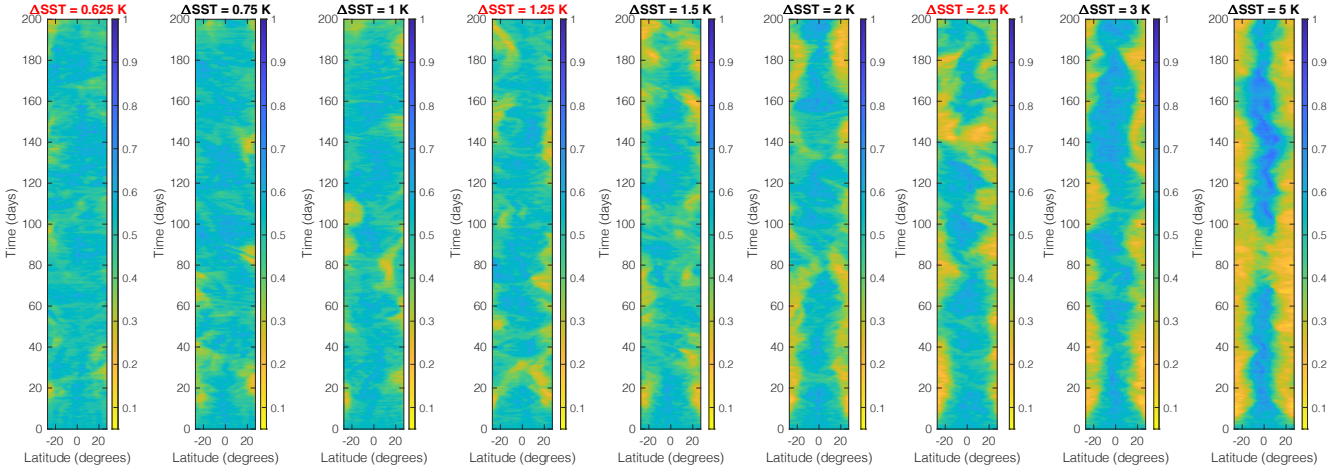

Figure 5. Hovmöller diagrams of column relative humidity averaged over 4° of longitude over the first 200 days of the simulations with $\langle SST \rangle$ = 300 and ΔSST = 0.625, 0.75, 1, 1.25, 1.5, 2, 2.5, 3, and 5 K, with CAM. The values of ΔSST that are required for RCEMIP-II are highlighted in red.

of atmospheric moisture content due to unpredictable convective interactions, as seen in similar simulations by Silvers and Robinson (2021) and speculated to be a result of parameterized convection.

The differences across different values of ΔSST is discussed below in Section 4.2, but here we note that all simulations display rich variability in the structure of the dry and moist regions (and convection). The SAM simulations in particular (Figure 4) depict disturbances that propagate along the long axis of the domain in both directions, with propagation speeds consistent with convectively coupled gravity waves. There are instances in which a dry band emerges from within a broader moist band, splitting the latter into two moist band, as well as instances in which two moist bands merge together. There is also lower frequency variability; for example, the location of the moist and dry regions in the SAM simulations with ΔSST = 0.625 K and ΔSST = 0.75 K oscillate back and forth with time. There are also fluctuations in the size of the moist, convective region, which contracts and expands along the long axis of the domain with a period of ∼30-40 days. This is most prominent in the SAM simulations with ΔSST = 2.5 K and ΔSST = 3 K but is also seen to a lesser extent in the CAM simulation at those values of ΔSST as well as both the SAM and CAM simulations at other values of ΔSST.

These low-frequency oscillations can have a substantial influence on domain mean quantities such as the top of atmosphere radiative fluxes (Figures 6 - 7). In the SAM simulations with strong SST gradients (Figure 6c), the OLR and net shortwave flux at the top of the atmosphere vary on ∼30 day time scales with amplitudes of $O(10)$ W m^{-2}. This behavior has also been seen in similar mock-Walker simulations with other CRMs, in which the amplitude of the fluctations can be larger (tens of W m^{-2}) depending on the model, microphysics settings, and other parameters (Guy Dagan, Andrew Williams, Peter Hill, Nick Lutsko, personal communication). Amongst the test simulations examined here with SAM and CAM, it seems that the oscillations are

https://doi.org/10.5194/gmd-2023-235
Preprint. Discussion started: 18 December 2023

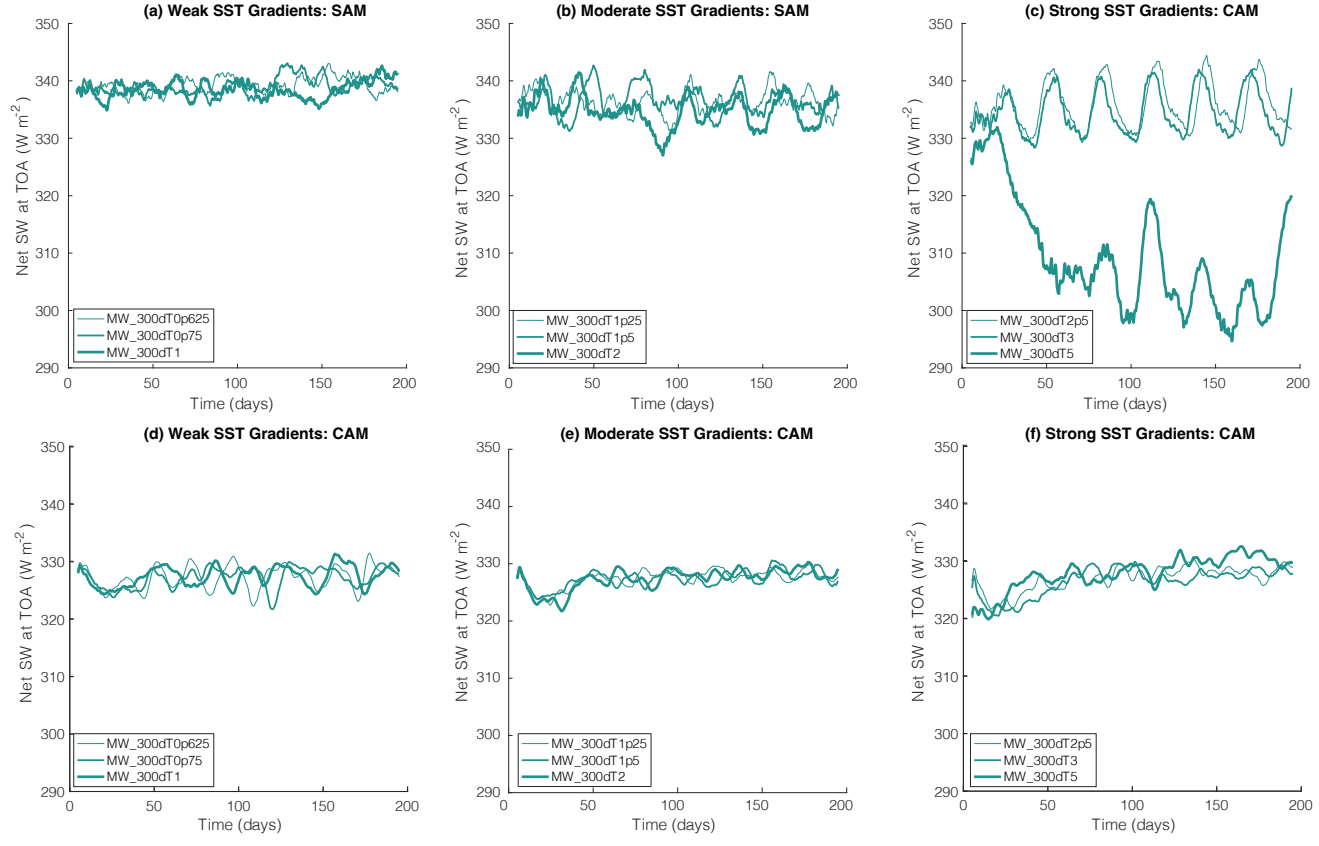

Figure 6. Domain mean net shortwave flux at the top of the atmosphere (W m^{-2}) in the simulations with (top row; panels a-c) SAM and (bottom row; panels d-f) CAM at $\langle SST \rangle$ = 300 K and (left column; panels a and d) weak (ΔSST = 0.625 K, 0.75 K, 1 K), (middle column; panels b and e) moderate (ΔSST = 1.25 K, 1.5 K, 2 K) and (right column; panels c and f) strong (ΔSST = 2.5 K, 3 K, 5 K) SST gradients. In each panel, a five-day running mean is shown with line thickness increasing with the value of ΔSST. Note that these SAM simulations, used to test the value of ΔSST, were performed with $SST(x) = \langle SST \rangle + \frac{\Delta SST}{2} cos\left(\frac{2\pi}{L_x}\left(x + \frac{L_x}{2}\right)\right)$ with λ = 6000 km and L_x = 6144 km, rather than Equation 1 and $\lambda = L_x$ as required for RCEMIP-II.

less extreme and less regular in CAM than they are in SAM (Figure 6). It is not clear whether this is due to the coarser grid spacing and parameterization of convection in CAM or its larger domain and spherical geometry.

We do not attempt to explain the origins of these low-frequency oscillations here, nor their dependence on $\langle SST \rangle$ and ΔSST. Their physical mechanisms and model dependence is a likely target of analysis across the full suite of RCEMIP-II simulations, once complete, and is thus beyond the scope of this protocol paper. In terms of defining the protocol, however, the presence of these low-frequency oscillations suggests that longer simulations than in RCEMIP-I (which consisted of 100 day simulations for the CRMs) will be needed to achieve robust equilibrium statistics in the RCEMIP-II mock-Walker configuration. Our test simulations indicate that simulations of at least 200 days in length for the CRMs, in which the first 75 days

https://doi.org/10.5194/gmd-2023-235
Preprint. Discussion started: 18 December 2023

Geoscientific Model Development
Discussions
Open Access
EGU

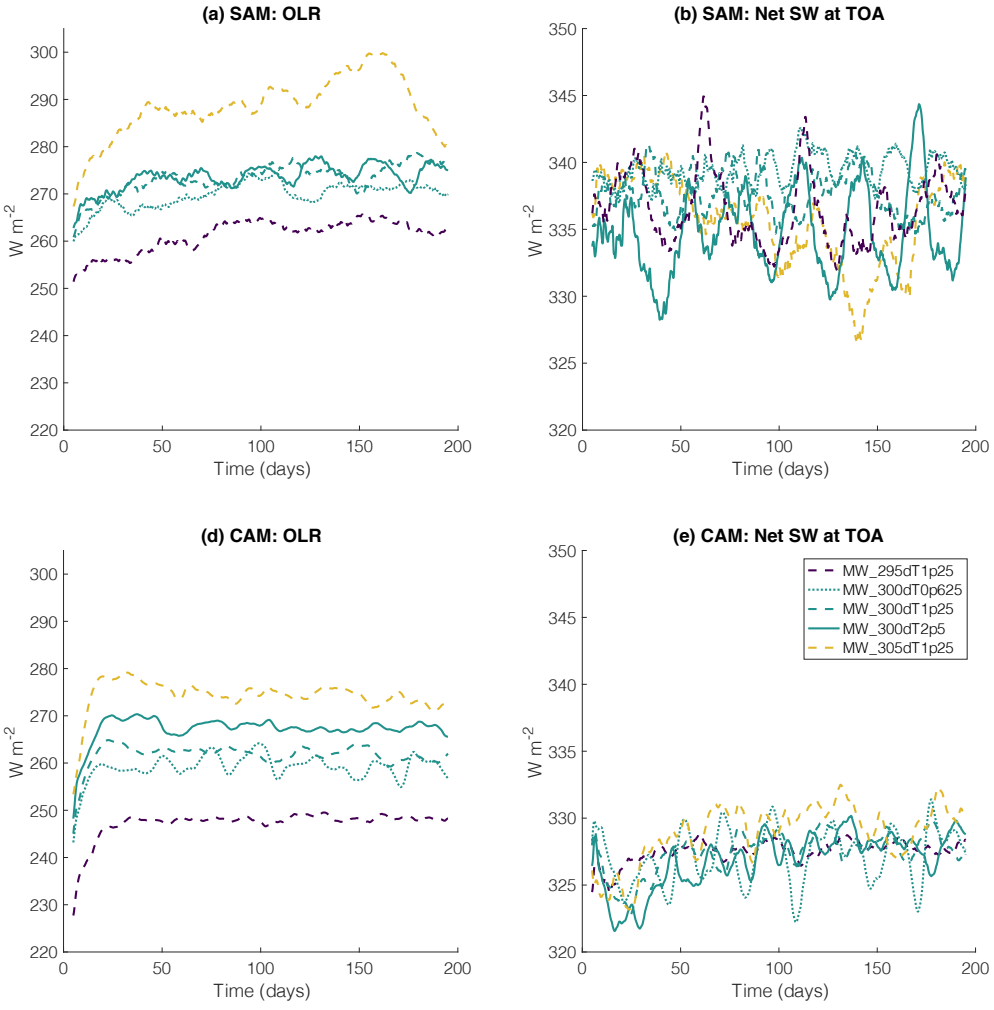

Figure 7. Domain mean (left column; panels a and c) outgoing longwave radiation (OLR; W m^{-2}) and (right column; panels b and d) net shortwave flux at the top of the atmosphere (W m^{-2}) in the simulations required for RCEMIP-II (`MW_295dT1p25`, `MW_300dT0p625`, `MW_300dT1p25`, `MW_300dT2p5`, and `MW_305dT1p25`) with (top row; panels a and b) SAM and (bottom row; panels c and d) CAM over the first 200 days of the simulation. A five-day running mean has been applied to all data, note the different axes in the left and right column.

https://doi.org/10.5194/gmd-2023-235
Preprint. Discussion started: 18 December 2023


Geoscientific Model Development Discussions

are excluded from the equilibrium averaging period, should be sufficient to average over multiple cycles of the ∼30 day oscillations and achieve robust statistics, while still being computationally feasible. If an individual model develops oscillations of even lower frequency, longer simulations with that model may be needed.

4.2 Sensitivity to ΔSST

Figures 4-5 indicate that the moist, convective region narrows and the range of CRH values in the domain increases as the SST gradient increases. SAM systematically exhibits a larger range of CRH values than CAM, though. The simulations tend to divide into three groups, with weak (ΔSST = 0.625, 0.75, and 1 K), moderate (ΔSST = 1.25, 1.5, and 2 K), and strong (ΔSST = 2.5, 3, and 5 K) SST gradients, though these groups are most distinct for SAM than CAM. In the group with weak SST gradients ((ΔSST = 0.625, 0.75, and 1 K) there are alternating moist and dry regions across the entire domain in the SAM simulation (Figure 4), reminiscent of the self-aggregation of convection seen in RCE simulations with the same geometry but uniform SST (Wing et al., 2020a). This suggests that $\Delta SST \leq$1 K provides such a weak SST gradient that the convection doesn't "care". The circulations set up by the intrinsic self-aggregation are thus stronger than those forced by the SST gradient. In the group with moderate SST gradients (ΔSST = 1.25, 1.5, and 2 K), there is typically one moist, convecting region centered over the warmest SSTs with some variability in its spatial extent. In these simulations, the SST gradient has forced a domain-spanning overturning circulation. In the group with strong SST gradients (ΔSST = 2.5, 3, and 5 K), stronger low-frequency oscillations emerge (particularly in SAM) and the convective region is increasingly narrow.

The low-frequency oscillations discussed above are quite regular in the SAM simulations with ΔSST = 2.5 and 3 K, but are more extreme and more irregular with ΔSST = 5 K. The `MW_300dT5` SAM simulation exhibits oscillations in the domain-mean net shortwave flux at the top of the atmosphere of up to ∼20 W m^{-2} but the magnitude varies (Figure 6c). This in part motivates us to avoid the use of such strong SST gradients in our selection of the required Phase II simulations. In the CAM simulations, the low-frequency oscillations are less prevalent and have less dependence on ΔSST (Figure 6). Another reason to exclude simulations with ΔSST = 5 K is that they, along with other simulations that have very warm SSTs in at least part of the domain (such as those with $\langle SST \rangle$ = 305 K) take longer to reach equilibrium, at least in SAM (Figures 6-7). `MW_305dT1p25` is a required simulation, but at least in this particular model, simulations longer than 200 days may be required for it to reach equilibrium.

Since the response of clouds to warming is one of the themes of RCEMIP, we also examine the sensitivity of cloud amount to the prescribed ΔSST. Figure 8 shows cloud fraction profiles for ΔSST = 0.625 K, 1.25 K, and 2.5 K, as well as the corresponding `RCE_large` simulations from RCEMIP-I, with uniform SST (ΔSST = 0 K) for reference. The dependencies of cloud fraction on ΔSST generally hold across the entire set of ΔSST values examined, not just those shown in Figure 8. In SAM, increasing ΔSST increases the low cloud fraction due to the presence of colder SSTs and stronger subsidence in the cold region. A more nuanced examination of clouds using ISCCP histograms demonstrated that the SAM mock-Walker simulations have more numerous, thicker, deeper low clouds (perhaps indicative of stratocumulus) than their RCEMIP-I counterparts with uniform SST (Stauffer, 2023). Increasing ΔSST also tends to decrease the high cloud fraction. In CAM, ΔSST has little effect on low clouds, except perhaps in the simulations at $\langle SST \rangle$ = 295 K (Figure 8d). As in SAM, increasing ΔSST decreases the

https://doi.org/10.5194/gmd-2023-235
Preprint. Discussion started: 18 December 2023

Geoscientific Model Development Discussions
Open Access
EGU

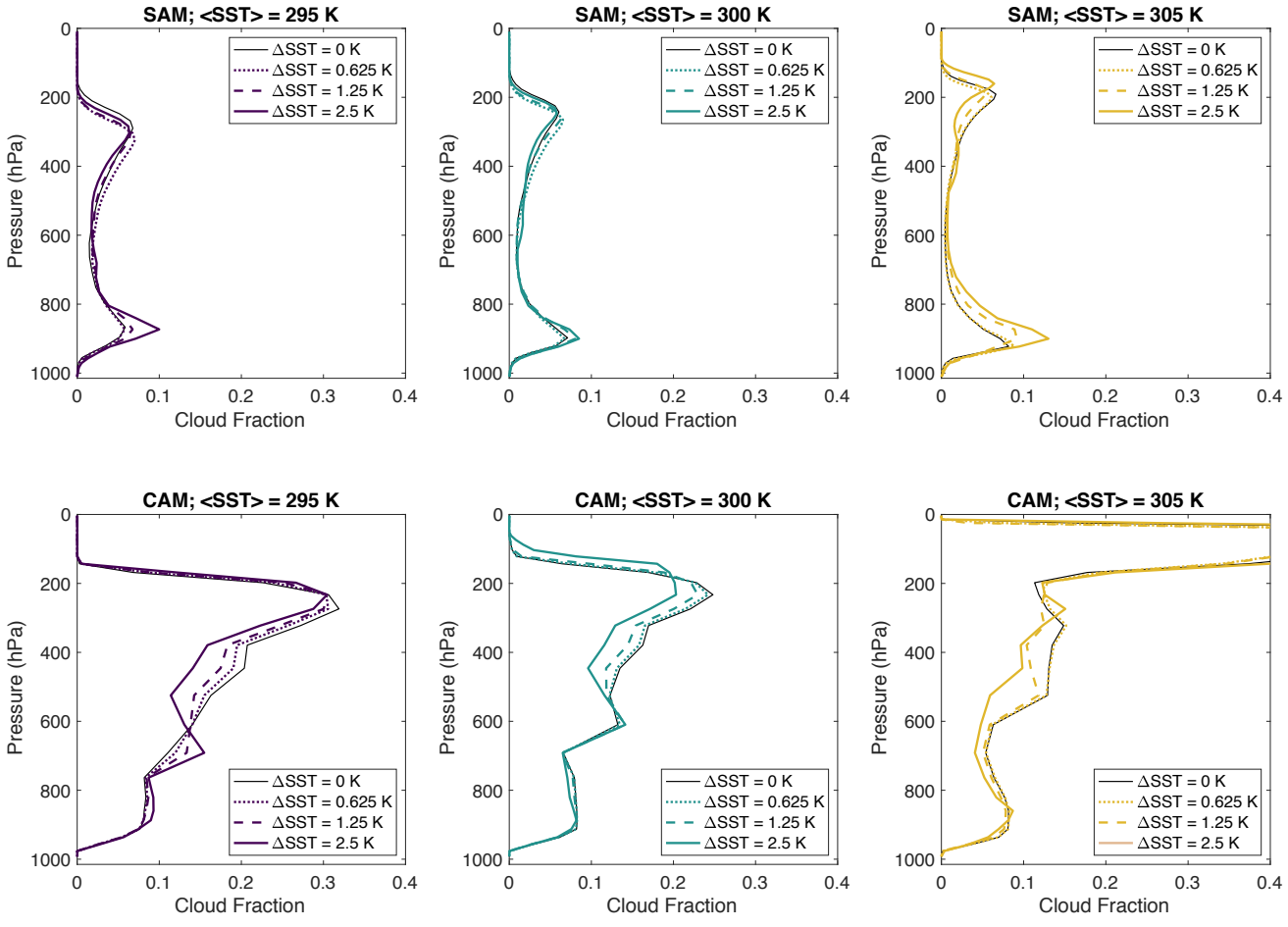

Figure 8. Domain- and time- mean profiles of cloud fraction, excluding the first 100 days of simulation, for simulations with $\langle SST \rangle$ of (left) 295, (middle) 300, and (right) 305 K. The corresponding `RCE_large` simulations from RCEMIP-I, with uniform SST (ΔSST = 0 K) are plotted in the solid black line. The line style indicates the value of ΔSST (see legend).

high cloud fraction in CAM (Figure 8), except in those simulations with $\langle SST \rangle$ = 305 K (Figure 8f), which have much larger high cloud fractions (~ 0.8) that tend to increase with increasing ΔSST (not shown). CAM6 is known to generate a lot of thin, high clouds over warm SSTs in RCEMIP-I (Reed et al., 2021), which is seen also here in RCEMIP-II.

The response of clouds to warming is similar across all values of ΔSST (Figure 8). The upward shift and decrease in high cloud fraction is robust and consistent with the response in the RCEMIP-I simulations with uniform SST (Stauffer and Wing, 2022). There is some suggestion of an increase in low cloud fraction with warming, particularly in SAM. A detailed calculation of the cloud feedback using cloud radiative kernels and its decomposition into contributions from changes in cloud amount,

https://doi.org/10.5194/gmd-2023-235
Preprint. Discussion started: 18 December 2023


Geoscientific Model Development Discussions

altitude, and optical depth indicated that the SAM mock-Walker simulations have cloud feedbacks of the same sign but larger magnitudes than their RCEMIP-I counterparts (Stauffer, 2023).

4.3 Sensitivity to Domain Size

The test simulations with SAM described above follow the domain configuration for CRMs specified in Section 3.2.1. The domain is the same as that used for the SAM `RCE_large` simulations in RCEMIP-I; there are 2048 x 128 grid points in the horizontal with a grid spacing of 3 km, resulting in a horizontal domain that is 6144 km x 384 km, or an aspect ratio of 16:1. There are 74 vertical levels following Table 3 of Wing et al. (2018). The experimental design for RCEMIP-II calls for the domain configuration to be the same as in RCEMIP-I, to allow for a clean comparison as well as keep the simulations computationally inexpensive. However, the results could be sensitive to both the long and short dimensions of the domain. For example, prior mock-Walker studies have found that the structure of precipitation and vertical profiles of cloudiness are sensitive to the long dimension of the domain (Silvers and Robinson, 2021; Bretherton et al., 2006). In order to provide some context for the results in our chosen domain configuration, we performed a few test simulations with SAM with different domain sizes: (1) A `wide` domain, which is twice as big in the short dimension and has an aspect ratio of 8:1 (2048 x 256 grid points; 6144 km x 768 km); (2) A `long` domain, which is twice as big in the long dimension and has an aspect ratio of 32:1 (4096 x 128 grid points; 12,288 km x 384 km); and (3) A long and wide (`longwide`) domain, which is twice as big in both dimensions so has the same 16:1 aspect ratio as the control simulation (4096 x 256 grid points; 12,288 km x 768 km). All simulations used to test the domain size utilize $SST(x) = \langle SST \rangle + \frac{\Delta SST}{2} cos\left(\frac{2\pi}{L_x}\left(x + \frac{L_x}{2}\right)\right)$ with λ = 6000 km and L_x = 6144 km, rather than Equation 1 and $\lambda = L_x$ as required for RCEMIP-II. The `long` and `longwide` simulations include two wavelengths of the SST pattern, but maintain the same SST gradient as the control domain. We conduct these domain size sensitivity tests for the `MW_300dT1p25` and `MW_300dT2p5` simulations (`longwide` is only performed for the `MW_300dT1p25` simulation).

The `MW_300dT1p25wide` and `MW_300dT2p5wide` simulations exhibit similar spatial structures of convection to that in their narrower counterparts (`MW_300dT1p25` and `MW_300dT2p5`), as seen in the CRH field in Figures 9-10, as well as the precipitation, OLR, and vertical velocity fields (not shown). The wide simulations are able to fit more convective cells across their short dimension, but otherwise the convection is similarly confined to the warmest SSTs and exhibits a similar temporal evolution (Figures 9a,b and 10a,b). This indicates that, at least in this situation with doubly periodic boundary conditions, mock-Walker simulations with different domain widths but the same domain length exhibit qualitatively similar behaviors. When comparing the `MW_300dT1p25longwide` simulation to the `MW_300dT1p25long` simulation, the spatial structures are also generally similar, though it takes longer for the `MW_300dT1p25longwide` to evolve to match the `MW_300dT1p25long` simulation.

The `MW_300dT2p5long` simulation exhibits similar spatial structures and temporal evolution of convection to that in its shorter counterpart `MW_300dT2p5`, except the pattern is repeated twice (Figure 10a,c). That is, the moist convecting regions are confined to the regions with warmest SSTs at the middle and left and right edges of the domain. There are a few differences: the central warm region is not quite as uniformly moist in the `long` simulation, and the low-frequency oscillations in the size

https://doi.org/10.5194/gmd-2023-235
Preprint. Discussion started: 18 December 2023

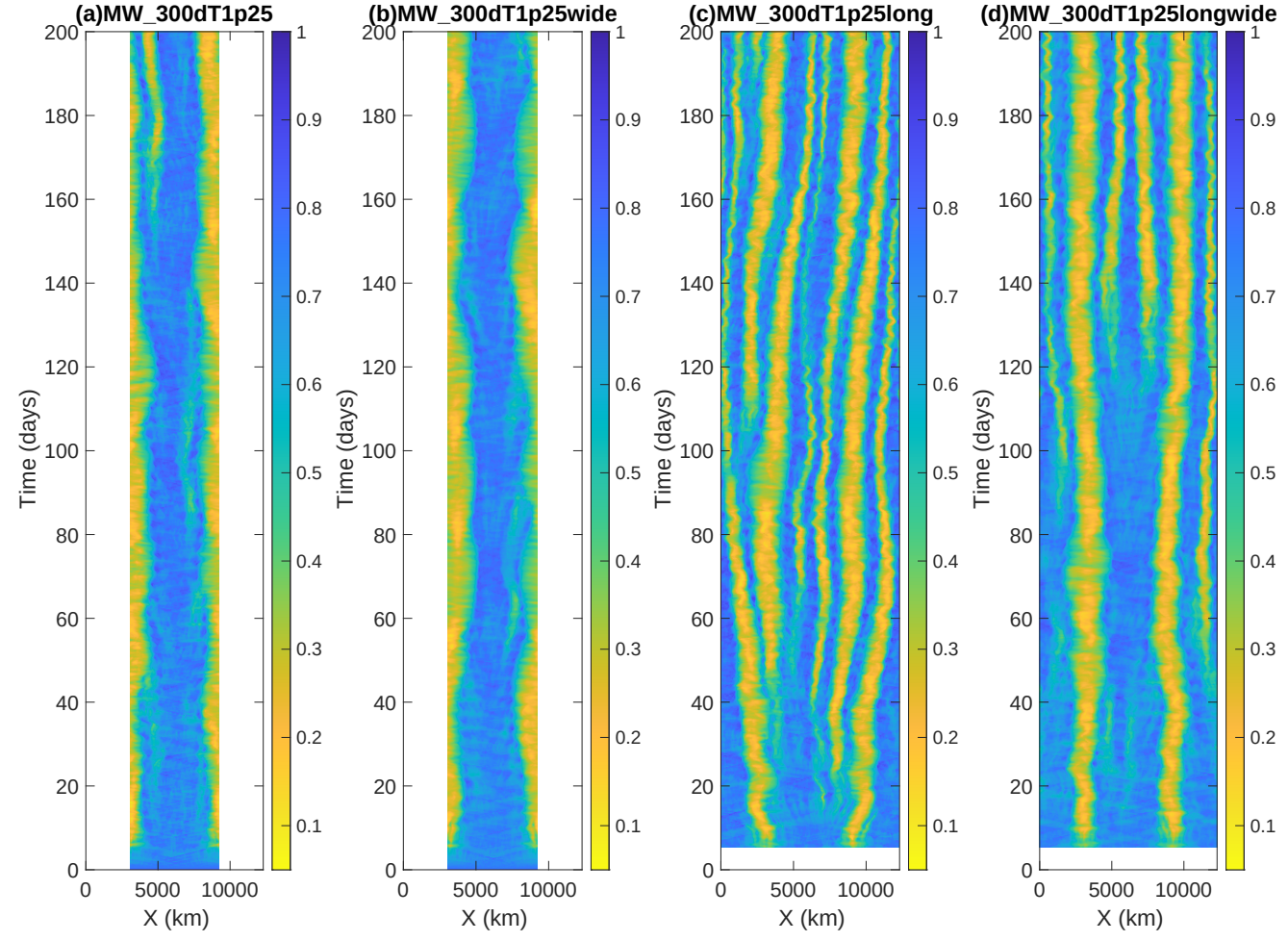

Figure 9. Hovmöller diagrams of y-averaged column relative humidity in the `MW_300dT1p25` simulation with SAM for (a) the standard domain size, (b) a domain that is twice as wide in the y-dimension, (c) a domain that is twice as long in the x-dimension, and (d) a domain that is twice as wide and twice as long. Note that these SAM simulations, used to test the domain size, were performed with $SST(x) = \langle SST \rangle + \frac{\Delta SST}{2} cos\left(\frac{2\pi}{L_x}\left(x + \frac{L_x}{2}\right)\right)$ with λ = 6000 km and L_x = 6144 km, rather than Equation 1 and $\lambda = L_x$ as required for RCEMIP-II.

https://doi.org/10.5194/gmd-2023-235
Preprint. Discussion started: 18 December 2023

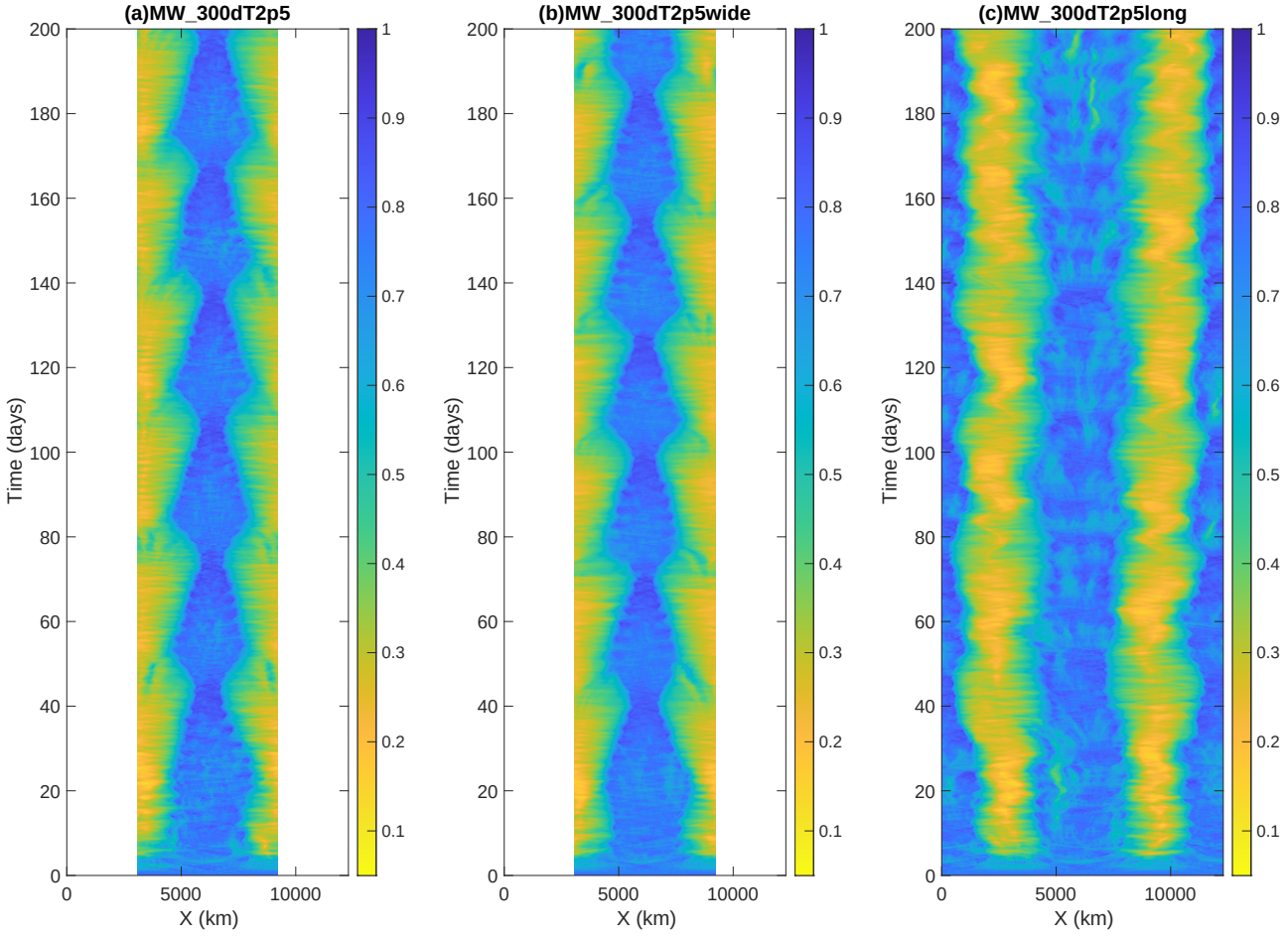

Figure 10. Hovmöller diagrams of y-averaged column relative humidity in the `MW_300dT2p5` simulation with SAM for (a) the standard domain size, (b) a domain that is twice as wide in the y-dimension, (c) a domain that is twice as long in the x-dimension. Note that these SAM simulations, used to test the domain size, were performed with $SST(x) = \langle SST \rangle + \frac{\Delta SST}{2} cos\left(\frac{2\pi}{L_x}\left(x + \frac{L_x}{2}\right)\right)$ with λ = 6000 km and L_x = 6144 km, rather than Equation 1 and $\lambda = L_x$ as required for RCEMIP-II.

https://doi.org/10.5194/gmd-2023-235
Preprint. Discussion started: 18 December 2023

Geoscientific Model Development Discussions
Open Access
EGU

of the moist region are less notable. However, to first order, the `MW_300dT2p5long` simulation appears to be an extension of the `MW_300dT2p5` simulation for another wavelength.

The `MW_300dT1p25long` simulation, however, has quite different behavior than its shorter counterpart (`MW_300dT1p25`). Initially the moist convecting regions are confined to the regions with warmest SSTs, but unlike the control `MW_300dT1p25` simulation, this is not maintained in the `long` simulation (Figure 9a,c). Instead, convection and precipitation begin to also develop on the periphery of the warm SSTs and eventually, narrower bands emerge with no preference to occur over the regions of the domain where the SST is maximized. In this regard, the `MW_300dT1p25long` simulation is similar to the simulations with weaker SST gradients (i.e., `MW_300dT0p625`) and reminiscent of self-aggregation of convection with uniform SST. This domain length dependence is similar to that found in the mock-Walker simulations of Silvers and Robinson (2021), though in their longer simulations they utilized the same ΔSST between the center of the domain and the edges, resulting in a weaker SST gradient. Thus, it is somewhat surprising that the breakdown of convection into narrow bands spanning the whole domain occurs in our long simulation, in which the SST gradient is unchanged. It suggests that ΔSST = 1.25 K is near the threshold for when the circulation forced by the SST gradient is strong enough to overcome those of intrinsic self-aggregation, and when provided by a longer domain with multiple wavelengths of SST, intrinsic self-aggregation outweighs the forced circulation. In the `MW_300dT1p25` simulation with the control domain size, there is also some suggestion that convection is beginning to break down into narrower bands right at the end of the simulation (Figure 9a), so if given enough time that simulation may also evolve to be dominated by intrinsic self-aggregation. In the the `MW_300dT1p25longwide` simulation, the moist convecting regions are confined to the regions with warmest SSTs for the first $\sim$100 days of the simulation, but they eventually breakdown into narrow bands spanning the whole domain as in `MW_300dT1p25long` (Figure 9c,d).

Despite the differences in convective structures discussed above, the simulations with different domain sizes generally have similar mean statistics (Figure 11). The `wide` simulations at both ΔSST = 1.25 K and ΔSST = 2.5 K have similar mean values and temporal variability as their narrower counterparts. The `MW_300dT2p5long` simulation has lower amplitude and somewhat less regular, lower amplitude low-frequency oscillations than its shorter counterpart, though roughly similar mean values. The precipitable water in the `MW_300dT1p25long` and `MW_300dT1p25longwide` simulations diverges to much lower values than their shorter counterparts, as higher fractions of the domain are occupied by dry areas. Consistent with the lower precipitable water, the OLR also tends to be higher in these simulations.

5 Discussion and Next Steps

In summary, a mock-Walker configuration with a specified, sinusoidal SST boundary condition is proposed for RCEMIP-II. This is intended to provide a partial constraint on convection and circulation that is hypothesized to narrow the intermodel spread while still allowing for rich interactions between convection, clouds, and circulations. RCEMIP-II will build on the success of RCEMIP-I to facilitate deeper understanding of cloud-circulation coupling and convective aggregation and its role in climate.

https://doi.org/10.5194/gmd-2023-235
Preprint. Discussion started: 18 December 2023

Geoscientific Model Development
Discussions
Open Access
EGU

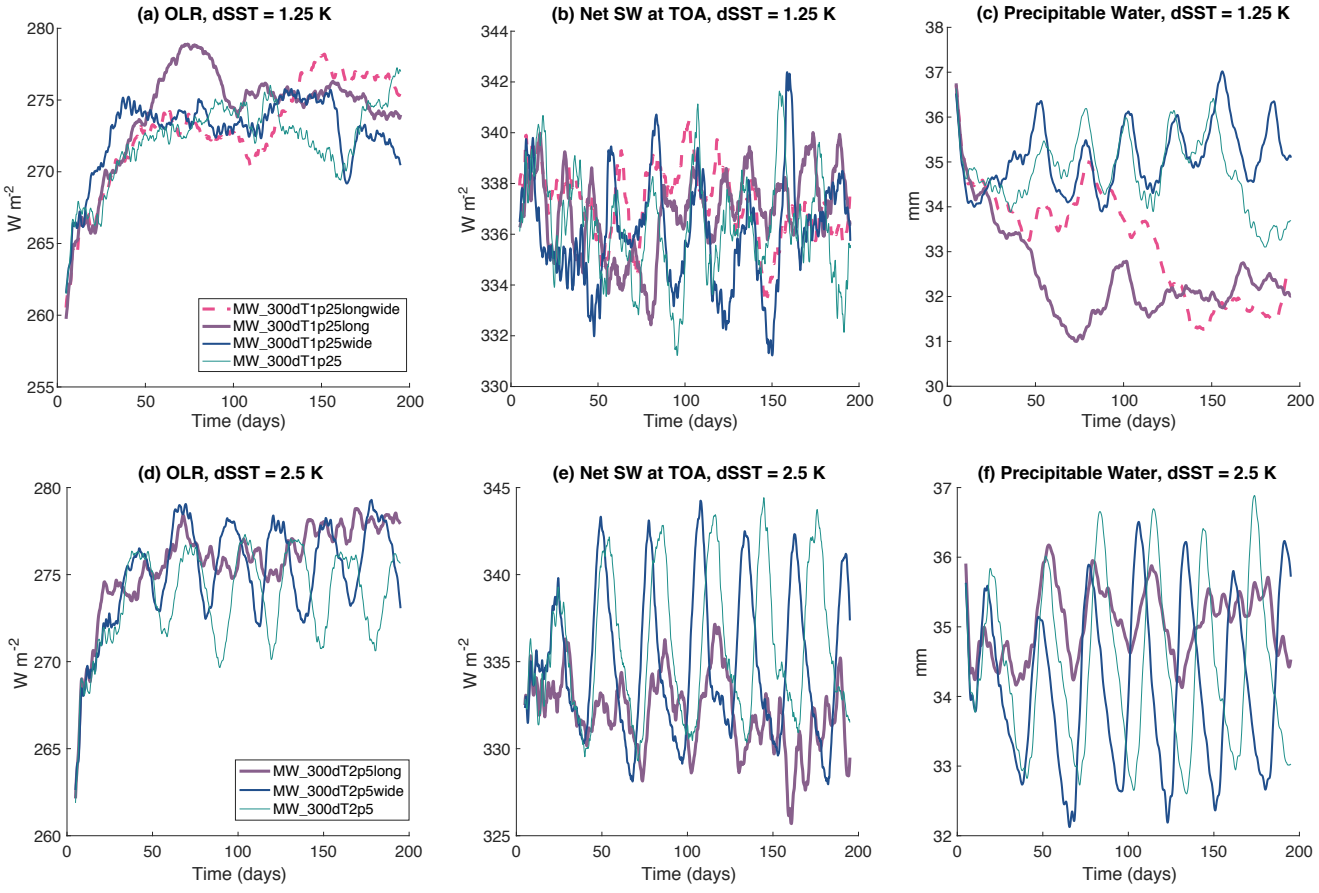

Figure 11. Domain mean (left column; panels a and d) outgoing longwave radiation (OLR; W m^{-2}), (middle column; panels b and e) net shortwave flux at the top of the atmosphere (W m^{-2}), and (right column; panels c and f) precipitable water (mm) in simulations with SAM with $\langle SST \rangle$ = 300 K and (top row; panels a-c) ΔSST = 1.25 K and (bottom row; panels d-f) ΔSST = 2.5 at different domain sizes. The domain sizes include the standard domain size (thin teal solid line), a domain that is twice as wide (medium blue solid line), a domain that is twice as long (thick purple solid line), and a domain that is both twice as wide and twice as long (thick pink dash-dotted line). A five-day running mean has been applied to all data. Note that these SAM simulations, used to test the domain size, were performed with $SST(x) = \langle SST \rangle + \frac{\Delta SST}{2} cos\left(\frac{2\pi}{L_x}\left(x + \frac{L_x}{2}\right)\right)$ with λ = 6000 km and L_x = 6144 km, rather than Equation 1 and $\lambda = L_x$ as required for RCEMIP-II.

https://doi.org/10.5194/gmd-2023-235
Preprint. Discussion started: 18 December 2023


Geoscientific Model Development Discussions

After testing several equations for the SST boundary condition and nine different values of ΔSST with both SAM, a CRM, and CAM, a GCM, we selected five experiments to be required for RCEMIP-II (Table 1, Figure 1) with the experimental design as described in Section 3. The protocol is designed to allow for comparison between CRMs on a limited-area cartesian domain and GCMs on the global sphere. The selection of the required ΔSST values balances similarity to observed SST gradients in the equatorial Pacific and Atlantic with choices that, in our test simulations, exhibit different spatial structures of convection and circulation. As was the philosophy for RCEMIP-I, the set of five required simulations for RCEMIP-II was carefully selected to facilitate addressing the scientific objectives while minimizing the computational expense (and thus maximizing participation). The SST boundary condition is the only difference in the set-up between RCEMIP-II and RCEMIP-I. While this enables comparison between RCEMIP-I and RCEMIP-II, we welcome participation in RCEMIP-II from models that did not participate in RCEMIP-I.

In addition to providing example results for the five required RCEMIP-II simulations, we also test the sensitivity to ΔSST and the domain geometry. As ΔSST increases, the moist, convective region narrows and becomes increasingly confined to the warmest SSTs. With small values of ΔSST, there are alternating moist and dry region across the entire domain, reminiscent of the self-aggregation of convection seen in RCE simulations with uniform SST. At larger values of ΔSST, low-frequency oscillations in the extent of the moist, convective region and associated variability in domain mean quantities emerge. While low cloud fraction tends to increase and high cloud fraction tends to decrease with increasing ΔSST, the response of clouds to warming is similar across all values of ΔSST. Simulations with different domain sizes generally have similar mean statisics. The convective structures are relatively insensitive to the width (short horizontal dimension) of the CRM domain, but can be sensitive to the length (long horizontal dimension), depending on the value of ΔSST.

The breakdown to self-aggregated convection that spans the entire domain with longer time or larger length simulations (Section 4.3) is a potential concern for the choice of ΔSST = 1.25 K as representing the moderate SST gradient regime in the set of required RCEMIP-II simulations. It is possible that in some models, the behavior ΔSST = 1.25 K could look similar to that in ΔSST = 0.625 K, as the transition between regimes is likely model dependent. While we considered instead selecting ΔSST = 0.75, 1.5, and 3 K as the set of required simulations, since ΔSST = 1.5 K might be more securely in the moderate SST gradient range than ΔSST = 1.25 K, differences across models are likely larger than those due to a 0.25K ΔSST difference. Our chosen ΔSST values of 0.625, 1.25, and 2.5 K result in SST gradients that are more symmetrically weaker and stronger than observed than the alternatives. Furthermore, in RCEMIP-I, SAM tended to be one of the most strongly self-aggregated models (Wing et al., 2020a), which could indicate that the dominance of intrinsic self-aggregation over the SST-forced circulation could hold to higher ΔSST values in SAM than in other models. Indeed, there is no guarantee that ΔSST= 0.625 will result in a self-aggregation-like regime in models that have weaker self-aggregation tendencies. While intermodel differences in which regime each ΔSST value belongs to may complicate analysis, identifying where these regime transitions occur across the spectrum of models is a goal of RCEMIP-II. To aid in this, while only the simulations listed in Table 1 are required, we encourage participants to conduct simulations at additional ΔSST values near regime transitions if possible.

https://doi.org/10.5194/gmd-2023-235
Preprint. Discussion started: 18 December 2023


Geoscientific Model Development Discussions
Open Access
EGU

In addition to the objectives related to the simulated mean state, the response of clouds to warming, and the role of convective aggregation in climate described in Section 2, and the analysis plans described in Section 3.5, there are numerous other avenues of investigation that could be explored in the full RCEMIP-II ensemble. By including both models with explicit convection and those with parameterized convection, RCEMIP-II maintains the ability to determine how behavior depend on the representation of convection. Other possible lines of inquiry include determining the physical mechanisms leading to low-frequency oscillations and their dependence on ΔSST and investigating what controls the transition between weak, moderate, and strong SST gradient regimes.

In addition to the RCEMIP-II mock-Walker simulations described here, other community efforts utilizing the RCEMIP set-up to investigate other questions have been proposed. One effort involves repeating the RCEMIP-I simulations with aerosol-cloud interactions, to compare the response of clouds to aerosol perturbations at equilibrium under a wide range of SST values (RCEMIP-ACI). Such simulations could also be performed using the RCEMIP-II protocol to investigate aerosol-cloud interactions in the presence of a forced circulation. There has also been some interest in performing RCE (uniform thermal forcing) simulations with global models with rotation, which would generate convectively-coupled equatorial waves and tropical cyclones. In this way, the RCEMIP-I and RCEMIP-II protocols can be a foundation upon which auxiliary investigations with modified experimental designs can be built. A potential future phase III of RCEMIP could focus on adding a slab mixed layer and interactive SST to the RCEMIP-I and RCEMIP-II configurations. This would allow the convective aggregation and cloud-circulation coupling to be influenced by ocean-atmosphere interactions, which is one of the primary physical processes currently missing from the RCEMIP set-up.

Table 2 shows a preliminary list of models that intend to contribute to RCEMIP-II. It includes 17 models that participated in RCEMIP-I and 4 models that did not. This list may grow with participation from additional modeling groups and scientists across the world. We also welcome multiple configurations of a given model (i.e., the same model with various microphysics schemes). Appendix A details the output specification for RCEMIP-II, which closely follows that of RCEMIP-I with a few changes and additions. The additions are requested to faciliate analysis that was not possible with the RCEMIP-I data, and are divided into required and optional output requests.

Code availability. Analysis scripts used to generate the figures are available on GitHub at https://github.com/allison-wing/RCEMIP-II during the review process and will be archived in Zenodo upon publication. The version of the System for Atmospheric Modeling (Khairoutdinov and Emanuel, 2013) used here is publicly available at http://rossby.msrc.sunysb.edu/~marat/SAM/sam6.11.2_AWing.tar.gz and CAM6 is publicly available as part of CESM2 at https://github.com/ESCOMP/CESM/releases/tag/release-cesm2.1.3.

Data availability. Model configuration files and a subset of the model data needed to reproduce the figures is available in a Zenodo archive at https://doi.org/10.5281/zenodo.10137266 (Wing and Silvers, 2023). We thank the German Climate Computing Center (DKRZ) for hosting the standardized RCEMIP-I data (Wing et al., 2020b), which is publicly available online at http://hdl.handle.net/21.14101/

https://doi.org/10.5194/gmd-2023-235
Preprint. Discussion started: 18 December 2023

Geoscientific Model Development Discussions

Table 2. Preliminary list of models planning to participate in RCEMIP-II.

Model Type	Model	
CRM	DAM	Das Atmosphaerisch Modell (Romps, 2008)
CRM	FV3	GFDL-FV3 CRM (Zhou et al., 2019)
CRM	ICON	ICOsahedral Nonhydrostatic Model - Sapphire (Hohenegger et al., 2023)
CRM	MESO-NH	MESO-NH v5.6 (Lac et al., 2018)
CRM	UKMO-RA1-T	UK Met Office Idealized Model v11.0 (Stratton et al., 2018)
CRM	SAM-1MOM	System for Atmospheric Modeling, 1-moment microphysics (Khairoutdinov and Randall, 2003)
CRM	SAM-M2005	System for Atmospheric Modeling, M2005 microphysics (Morrison et al., 2005)
CRM	SAM-P3ice	System for Atmospheric Modeling, P3ice microphysics (Morrison and Milbrandt, 2015; Gasparini et al., 2022)
CRM	SCALE	Scalable Computing for Advanced Library and Environment v5.2.5 (Nishizawa et al., 2015; Sato et al., 2015)
CRM	VVM	Vector Vorticity Model (Wu et al., 2019)
GCRM	ICON	ICOsahedral Nonhydrostatic Model - Sapphire (Hohenegger et al., 2023)
GCRM	NICAM	Non-hydrostatic Icosahedral Atmospheric Model v16.3 (Satoh et al., 2014)
GCRM	SAM	Global System for Atmospheric Modeling (Khairoutdinov et al., 2022)
GCM	FV3-AM4	GFDL-FV3 with AM4 Physics (Zhao et al., 2018a, b)
GCM	CAM5	Community Atmosphere Model version 5 (Neale et al., 2012)
GCM	CAM6	Community Atmosphere Model version 6 (Danabasoglu et al., 2020)
GCM	CNRM-CM6	CNRM-CM6-1 - Atmosphere component (Roehrig and coauthors, 2020; Voldoire et al., 2019)
GCM	IPSL-CM6	LMDZ6A version (Hourdin and coauthors, 2020)
GCM	SP-CAM	Super-Parameterized Community Atmosphere Model (Randall et al., 2016)
GCM	UKMO-GA7.1	Met Office Unified Model Global Atmosphere v7.1 (Walters et al., 2019)

d4beee8e-6996-453e-bbd1-ff53b6874c0e. The standardized RCEMIP-II data will also be hosted and made publicly available in the DKRZ archive once all the RCEMIP-II simulations have been completed and submitted.

Appendix A: Output Specification

The RCEMIP-II output request closely follows that of RCEMIP-I, as described by (Wing et al., 2018) and its corresponding corrigendum. We highlight here a few variables to pay careful attention to and a few changes and additions.

A1 Output Variables

In all tables, the italicized variables are non-standard outputs, all others are standard CMIP6 output. Bolded variables are new compared to RCEMIP-I. The variables with a (-)^{l} symbol are outputs for GCMs only. The output should be "CMOR-ized", such that the output variable names and units are the same as in CMIP6, as listed in the below tables.

In addition to the listed variables, the horizontal coordinates, vertical coordinate, and time coordinate should also be output. The time coordinate should be in units of days since the beginning of the simulation. Output should be submitted on a x-y- (for CRMs) or latitude-longitude (for global models) grid. In the vertical, the variables should be on model levels and the necessary information to compute pressure on model levels should be provided. If your model does not employ pressure levels (i.e., it uses height levels or a type of hybrid level), please also output the domain- and time-mean values of pressure on your model levels, for approximate plotting purposes. Ideally this would be included in all files, but it is especially useful in the 1D files.

https://doi.org/10.5194/gmd-2023-235
Preprint. Discussion started: 18 December 2023


Geoscientific Model Development Discussions

CRMs should output all variables, including 3D variables, over the full simulation. GCMs should output 0D, 1D, 2D variables over the full simulation and 3D variables over last 200 days of simulation. GCRMs should output all variables over the full simulation, but only upload 0D, 1D, and 2D variables to the RCEMIP data respository (3D variables should be archived locally). **Note that the 3D output request is different than RCEMIP-I.**

Tables A1-A4 list the *required output*. Table A1 indicates the list of zero-dimensional domain-averaged variables (functions of t only) that are to be computed and output as hourly averages. Table A2 indicates the list of one-dimensional domain-averaged profiles (functions of z and t) that are to be computed and output as hourly averages. Table A3 indicates the list of two-dimensional variables (functions of x, y, and t) to output, as hourly averages. All models should output *tabot, uabot*, and *vabot* (the air temperature, eastward wind, and northward wind, respectively, at the lowest model level). Those models which routinely estimate and output 2m air temperature, 10m eastward wind, and 10m northward wind (*tas, uas*, and *vas*, respectively), should also output those variables. Models that use height coordinates should output vertical velocity, *wa500*, whereas models that use pressure-based coordinates should output omega, *wap500*. Table A4 indicates the list of three-dimensional variables to output, as instantaneous 6-hourly snapshots. Models that use height coordinates should output vertical velocity, *wa*, and pressure, *pa*, whereas models that use pressure-based coordinates should output omega, *wap*, and geopotential height *zg*.

Tables A5 lists *optional, but recommended output*, which consists of one 3-D variable to be output as 6-hourly instantaneous snapshots, two 2-D variables to be output as 30-minute instantaneous snapshots (in contrast to the hourly averages requested in Table A3) and four 2-D variables associated with the frozen moist static energy (FMSE) budget. The 30-minute instantaneous output will facilitate tracking of mesoscale convective systems and the FMSE budget output will facilitate diagnosing physical mechanisms of convective aggregation. *tntm*, the tendency of air temperature due to microphysical latent heating, is a new optional 3-D output to facilitate heat budget analysis. This is the term $L(c-e)$ where c is the condensation rate and e is the evaporation rate. **The optional requests for *tntm* and the 30-minute instantaneous 2-D variables are new compared to RCEMIP-I.**

A2 Cloud fraction

We request the diagnosis of a global cloud fraction profile (*cldfrac_avg*) that includes all clouds and is the fraction of the entire domain covered by cloud at a given height (Table A2). This 1-D variable should be a function of vertical level and time. Following Stauffer and Wing (2022), the presence of a cloud in CRMs (or models without a cloud scheme) should be defined where the mixing ratio of the total cloud condensate (cloud liquid water + cloud ice) is greater than 1 x 10^{-5} g g^{-1}. **Note that this is different from the original RCEMIP-I definition in Wing et al. (2018)**. GCMs or other models with cloud schemes should continue to provide the cloud fraction as output from the cloud scheme. For GCMs, we also request the output of a total cloud fraction for each grid column as the 2-D variable *cl*, which is a function of x,y, and t (Table A3), as well as the output of cloud fraction for each grid column as a function of height, as the 3-D variable *cldfrac*, which is a function of x, y, t, and vertical level (Table A4). Please output cloud fraction as a fraction (between 0 and 1), not a percentage out of 100. **The request of the 3-D variable *cldfrac* for GCMs is new compared to RCEMIP-I**.

https://doi.org/10.5194/gmd-2023-235
Preprint. Discussion started: 18 December 2023


Geoscientific Model Development Discussions
Open Access
EGU

A3 Cloud water variables

Following the conventions of CMIP6 (see http://clipc-services.ceda.ac.uk/dreq/index.html for variable descriptions), several of the cloud water variables have confusing variable names. The 0-D variable *clwvi_avg* (Table A1 and the 2-D variable *clwvi* (Table A3) represent the condensed water path which includes both cloud ice and cloud liquid water. The 1-D variable *clw_avg* (Table A2) and the 3-D variable *clw* (Table A4) represent only the cloud liquid water.

A4 Relative humidity

When computing relative humidity (the 1-D variable *hur_avg*, Table A2), care should be taken to compute the saturation with respect to liquid for temperatures above freezing and with respect to ice for temperatures below freezing. The formulas for saturation vapor pressure should follow those used in a given model's thermodynamics. If the model's thernodynamics interpolates between saturation over liquid and saturation over ice for temperatures near freezing, that should also be followed.

A5 Radiative heating rates and fluxes

The tendency of air temperature due to shortwave and longwave radiative heating assuming clear-sky should be output as 3-D variables (*tntrscs*, *tntrlcs*), in addition to the total radiative heating tendencies (*tntrs*, *tntrl*); see Table A4. **The request of the 3-D variables *tntrscs* and *tntrlcs* is new compared to RCEMIP-I**. The domain average shortwave and longwave radiative heating rate profiles should also be output as 1-D variables for all-sky and clear-sky conditions (*tntrs_avg*, *tntrl_avg*, *tntrscs_avg*, *tntrlcs_avg*; see Table A2). The downwelling and upwelling shortwave and longwave radiative fluxes, at the surface and top of atmosphere, and for all-sky and clear-sky conditions, are requested as 2-D variables (Table A3).

A6 CFMIP Observational Simulator Package (COSP)

COSP simulator outputs are requested for the ISCCP simulator, for GCMs that have COSP available as a diagnostic package. This will facilitate comparison with observations as well as the calculation and decomposition of cloud feedbacks (Zelinka et al., 2012a, b, 2013). More information about COSP can be found on the COSP website (https://cfmip.github.io). The ISCCP simulator provides pseudo-retrievals of cloud top pressure (CTP) and cloud optical thickness (tau) (Klein and Jakob, 1999; Webb et al., 2001). The following ISCCP simulator outputs are requested: hourly averages of ISCCP 2-D diagnostics (*cltisccp*: cloud fraction, *albisccp*: cloud albedo, and *pctisccp*: cloud top pressure; see Table A3) and 6-hourly instantaneous diagnostics of the ISCCP CTP-tau histograms (*clisccp*: cloud area percentage in the 7 pressure and 7 optical depth bins; see Table A4) . **The request for ISCCP simulator output for GCMs is new compared to RCEMIP-I**.

A7 Frozen Moist Static Energy Budget

Four optional 2D variables associated with the FMSE budget are requested in Table A5. If these variables (functions of x, y, and t) are diagnosed online in the model, their values may be output as hourly averages. If they are diagnosed offline from the instantaneous 3D output, they may be provided as instantaneous 6-hourly snapshots. For example, if *tnfmse*, the tendency of

https://doi.org/10.5194/gmd-2023-235
Preprint. Discussion started: 18 December 2023


Geoscientific Model Development Discussions
Open Access
EGU

FMSE, is diagnosed offline, it should be diagnosed from instantaneous *fmse* output. If it is diagnosed online from instantaneous variables, its hourly average can then be output.

FMSE is defined as $h = c_p T + gz + L_\mathrm{v} q - L_\mathrm{f} q_{ice}$. The values of c_p, g, L_v, and L_f used by the model formulation should be used to compute h. q_{ice} is the mass fraction of all ice phase condensates (cloud ice, snow, etc...). The mass-weighted vertical integral of FMSE is given by:

$$\widehat{h} = \int_0^{z_\mathrm{top}} (c_p T + gz + L_\mathrm{v} q - L_\mathrm{f} q_{ice})\, \rho \,\mathrm{d}z, \tag{A7}$$

or, in pressure coordinates,

$$\widetilde{h} = \frac{1}{g} \int_{p_\mathrm{top}}^{p_\mathrm{sfc}} (c_p T + gz + L_\mathrm{v} q - L_\mathrm{f} q_{ice})\, \mathrm{d}p. \tag{A8}$$

Care should be taken to make sure the same limits of integration are used at all times/locations. The mass-weighted vertical integral of the advective tendency of FMSE (*advfmse*) is given by

$$\int_0^{z_\mathrm{top}} \left(u\frac{\partial h}{\partial x} + v\frac{\partial h}{\partial y} + w\frac{\partial h}{\partial z} \right) \rho \,\mathrm{d}z. \tag{A9}$$

Ideally, FMSE would be diagnosed online and each model's advection scheme used to advect it. For instance, one could diagnose FSME from the prognostic variables just before and just after they are advected, and then the difference could be taken as a measure of the FMSE advective tendency. If this is not possible we ask that groups make their best effort to estimate these terms. The spatial variance of the mass-weighted vertical integral of frozen moist static energy is computed using the squared anomalies from the horizontal mean of the mass-weighted vertical integral of moist static energy ($\widehat{h}$). Its tendency (*tnfmsevar*) is given by

$$\frac{\partial}{\partial t} \left(\int_0^{z_\mathrm{top}} h \rho \,\mathrm{d}z \right)'^2 \tag{A10}$$

where $'$ indicates an anomaly from the horizontal mean.

https://doi.org/10.5194/gmd-2023-235
Preprint. Discussion started: 18 December 2023

Geoscientific Model Development Discussions
Open Access
EGU

Table A1. 0D hourly-averaged variables (t)

Variable Name	Description	Units
pr_avg	domain avg. suface precipitation rate	kg m^{-2} s^{-1}
hfls_avg	domain avg. surface upward latent heat flux	W m^{-2}
hfss_avg	domain avg. surface upward sensible heat flux	W m^{-2}
prw_avg	domain avg. water vapor path	kg m^{-2}
sprw_avg	domain avg. saturated water vapor path	kg m^{-2}
clwvi_avg	domain avg. condensed water path (cloud ice + cloud liquid)	kg m^{-2}
clivi_avg	domain avg. ice water path (cloud ice)	kg m^{-2}
rlds_avg	domain avg. surface downwelling longwave flux	W m^{-2}
rlus_avg	domain avg. surface upwelling longwave flux	W m^{-2}
rsds_avg	domain avg. surface downwelling shortwave flux	W m^{-2}
rsus_avg	domain avg. surface upwelling shortwave flux	W m^{-2}
rsdscs_avg	domain avg. surface downwelling shortwave flux - clear sky	W m^{-2}
rsuscs_avg	domain avg. surface upwelling shortwave flux - clear sky	W m^{-2}
rldscs_avg	domain avg. surface downwelling longwave flux - clear sky	W m^{-2}
rluscs_avg	domain avg. surface upwelling longwave flux - clear sky	W m^{-2}
rsdt_avg	domain avg. TOA incoming shortwave flux	W m^{-2}
rsut_avg	domain avg. TOA outgoing shortwave flux	W m^{-2}
rlut_avg	domain avg. TOA outgoing longwave flux	W m^{-2}
rsutcs_avg	domain avg. TOA outgoing shortwave flux - clear sky	W m^{-2}
rlutcs_avg	domain avg. TOA outgoing longwave flux -clear sky	W m^{-2}

https://doi.org/10.5194/gmd-2023-235
Preprint. Discussion started: 18 December 2023

Geoscientific Model Development Discussions
Open Access
EGU

Table A2. 1D hourly-averaged variables (z,t)

Variable Name	Description	Units
ta_avg	domain avg. air temperaure profile	K
ua_avg	domain avg. eastward wind profile	m s^{-1}
va_avg	domain avg. northward wind profile	m s^{-1}
hus_avg	domain avg. specific humidity profile	kg/kg
hur_avg	domain avg. relative humidity profile	%
clw_avg	domain avg. mass fraction of cloud liquid water profile	kg/kg
cli_avg	domain avg. mass fraction of cloud ice profile	kg/kg
plw_avg	domain avg. mass fraction of precipitating liquid water profile	kg/kg
pli_avg	domain avg. mass fraction of precipitating ice profile	kg/kg
theta_avg	domain avg. potential temperature profile	K
thetae_avg	domain avg. equivalent potential temperature profile	K
tntrs_avg	domain avg. shortwave radiative heating rate profile	K s^{-1}
tntrl_avg	domain avg. longwave radiative heating rate profile	K s^{-1}
tntrscs_avg	domain avg. shortwave radiative heating rate profile - clear sky	K s^{-1}
tntrlcs_avg	domain avg. longwave radiative heating rate profile - clear sky	K s^{-1}
cldfrac_avg	global cloud fraction profile	

https://doi.org/10.5194/gmd-2023-235
Preprint. Discussion started: 18 December 2023

Geoscientific Model Development Discussions
Open Access
EGU

Table A3. 2D hourly averaged variables (x,y,t)

Variable Name	Description	Units
pr	surface precipitation rate	kg m^{-2} s^{-1}
hfls	surface upward latent heat flux	W m^{-2}
hfss	surface upward sensible heat flux	W m^{-2}
rlds	surface downwelling longwave flux	W m^{-2}
rlus	surface upwelling longwave flux	W m^{-2}
rsds	surface downwelling shortwave flux	W m^{-2}
rsus	surface upwelling shortwave flux	W m^{-2}
rsdscs	surface downwelling shortwave flux - clear sky	W m^{-2}
rsuscs	surface upwelling shortwave flux - clear sky	W m^{-2}
rldscs	surface downwelling longwave flux - clear sky	W m^{-2}
rluscs	surface upwelling longwave flux - clear sky	W m^{-2}
rsdt	TOA incoming shortwave flux	W m^{-2}
rsut	TOA outgoing shortwave flux	W m^{-2}
rlut	TOA outgoing longwave flux	W m^{-2}
rsutcs	TOA outgoing shortwave flux - clear sky	W m^{-2}
rlutcs	TOA outgoing longwave flux -clear sky	W m^{-2}
prw	water vapor path	kg m^{-2}
sprw	saturated water vapor path	kg m^{-2}
clwvi	condensed water path (cloud ice + cloud liquid)	kg m^{-2}
clivi	ice water path (cloud ice)	kg m^{-2}
psl	sea level pressure	Pa
tas	2m air temperature	K
tabot	air temperature at lowest model level	K
uas	10m eastward wind	m s^{-1}
vas	10m northward wind	m s^{-1}
uabot	eastward wind at lowest model level	m s^{-1}
vabot	northward wind at lowest model level	m s^{-1}
wa500 or *wap500*	vertical velocity or omega at 500 hPa	m s^{-1} or Pa s^{-1}
cl[!]	total cloud fraction of grid column	
pr_conv[!]	surface convective precipitation rate	kg m^{-2} s^{-1}
albisccp[!]	ISCCP mean cloud albedo	
cltisccp[!]	ISCCP total cloud cover	%
pctisccp[!]	ISCCP mean cloud top pressure	Pa

https://doi.org/10.5194/gmd-2023-235
Preprint. Discussion started: 18 December 2023

Geoscientific Model Development Discussions
Open Access
EGU

Table A4. 3D instantaneous 6-hourly variables (x,y,z,t)

Variable Name	Description	Units
clw	mass fraction of cloud liquid water	g/g
cli	mass fraction of cloud ice	g/g
plw	mass fraction of precipitating liquid water	g/g
pli	mass fraction of precipitating ice	g/g
ta	air temperature	K
ua	eastward wind	m s^{-1}
va	northward wind	m s^{-1}
hus	specific humidity	g/g
wa or wap	vertical velocity or omega	m s^{-1} or Pa s^{-1}
pa or zg	pressure or geopotenial height	Pa or m
tntrs	tendency of air temperature due to shortwave radiative heating	K s^{-1}
tntrl	tendency of air temperature due to longwave radiative heating	K s^{-1}
tntrscs	tendency of air temperature due to shortwave radiative heating - clear sky	K s^{-1}
tntrlcs	tendency of air temperature due to longwave radiative heating - clear sky	K s^{-1}
cldfrac[!]	cloud fraction	
mc[!]	convective mass flux	kg m^{-2} s^{-1}
tntc[!]	tendency of air temperature due to moist convection	K s^{-1}
clisccp[!]	ISCCP cloud area percentage in optical depth and pressure bins	%

https://doi.org/10.5194/gmd-2023-235
Preprint. Discussion started: 18 December 2023

Geoscientific Model Development Discussions

Table A5. Optional output variables

Variable Name	Description	Units
6-hourly instantaneous 3-D variables (x,y,z,t)		
tntm	tendency of air temperature due to microphysical latent heating	K s^{-1}
30-minute instantaneous 2-D variables (x,y,t)		
rlut_inst	TOA outgoing longwave flux	W m^{-2}
pr_inst	surface precipitation rate	kg m^{-2} s^{-1}
Hourly 2-D variables (x,y,t)		
fmse	mass-weighted vert. integral of FMSE	J m^{-2}
advfmse	mass-weighted vert. integral of advective tendency of FMSE	J m^{-2} s^{-1}
tnfmse	tendency of mass-weighted vert. integral of FMSE	J m^{-2} s^{-1}
tnfmsevar	tendency of spatial variance of mass-weighted vert. integral of FMSE	J^2 m^{-4} s^{-1}

Author contributions. AAW led the writing of the text. AAW and LGS performed and analyzed simulations. All authors contributed to discussing the goals and specifications of RCEMIP-II and editing the text.

Competing interests. No competing interests are present.

Acknowledgements. AAW acknowledges support from NSF grants AGS-2140419 and AGS-1830724. LGS and KAR acknowledge support from NSF grant AGS-2327958. KAR was also partially supported by the Department of Energy Office of Science award number DE-SC0016605 "A Framework for Improving Analysis and Modeling of Earth System and Intersectoral Dynamics at Regional Scales" The authors thank Tim Cronin, Guy Dagan, Peter Hill, Nick Lutsko, Andrew Williams, and the participants of the RCEMIP breakout session at the 2023 CFMIP-GASS Meeting in Paris for helpful discussions, and to Catherine Stauffer for assistance with initial analysis of the test simulations. We also thank Jean-Pierre Chaboureau, Guy Dagan, Blaž Gasparini, Peter Hill, Cathy Hohenegger, Chris Holloway, Todd Jones, Marat Khairoutdinov, Shuhei Matsugishi, David Randall, Camille Risi, Romain Roehrig, David Romps, Masaki Satoh, Lorenzo Tomassini, Chien-Ming Wu, and Ming Zhao for agreeing to perform RCEMIP-II simulations with the models listed in Table 2. We also thank Marat Khairoutdinov for maintaining and providing the SAM cloud-resolving model, which was used to perform simulations in this paper.

https://doi.org/10.5194/gmd-2023-235
Preprint. Discussion started: 18 December 2023

Geoscientific Model Development Discussions

References

Back, L. E. and Bretherton, C. S.: On the relationship between SST gradients, boundary layer winds, and convergence over the tropical oceans, J. Climate, 22, 4182–4196, https://doi.org/10.1175/2009JCLI2392.1, 2009.

Becker, T. and Wing, A. A.: Understanding the extreme spread in climate sensitivity within the Radiative-Convective Equilibrium Model Intercomparison Project, J. Adv. Model. Earth Syst., 12, e2020MS002 165, 2020.

Bony, S., Stevens, B., Frierson, D. M. W., Jakob, C., Kageyam, M., Pincus, R., Shepherd, T. G., Sherwood, S. C., Siebesma, A. P., Sobel, A. H., Watanabe, M., and Webb, M. J.: Clouds, circulation and climate sensitivity, Nature Geoscience, 8, 261–268, https://doi.org/doi:10.1038/ngeo2398, 2015.

Bretherton, C. S. and Sobel, A. H.: A simple model of a convectively-coupled Walker circulation using the weak temperature gradient approximation, J. Climate, 15, 2907–2920, 2002.

Bretherton, C. S., Blossey, P. N., and Peters, M. E.: Interpretation of simple and cloud-resolving simulations of moist-convection-radiation interaction with a mock-Walker circulation, Theor. Comput. Fluid Dyn., 20, 421–442, https://doi.org/10.1007/s00162-006-0029-7, 2006.

Danabasoglu, G., Lamarque, J.-F., Bacmeister, J., Bailey, D. A., DuVivier, A. K., Edwards, J., Emmons, L. K., Fasullo, J., Garcia, R., Gettelman, A., Hannay, C., Holland, M. M., Large, W. G., Lauritzen, P. H., Lawrence, D. M., Lenaerts, J. T. M., Lindsay, K., Lipscomb, W. H., Mills, M. J., Neale, R., Oleson, K. W., Otto-Bliesner, B., Phillips, A. S., Sacks, W., Tilmes, S., van Kampenhout, L., Vertenstein, M., Bertini, A., Dennis, J., Deser, C., Fischer, C., Fox-Kemper, B., Kay, J. E., Kinnison, D., Kushner, P. J., Larson, V. E., Long, M. C., Mickelson, S., Moore, J. K., Nienhouse, E., Polvani, L., Rasch, P. J., and Strand, W. G.: The Community Earth Ssytem Model Version 2 (CESM2), J. Adv. Model. Earth Syst., 12, e2019MS001 916, https://doi.org/10.1029/2019MS001916, 2020.

Gasparini, B., Sokol, A. B., Wall, C. J., Hartmann, D. L., and Blossey, P. N.: Diurnal Differences in Tropical Maritime Anvil Cloud Evolution, J. Climate, 35, 1655–1677, 2022.

Grabowski, W. W., Yano, J.-I., and Moncrieff, M. W.: Cloud resolving modeling of tropical circulations driven by large-scale SST gradients, J. Atmos. Sci., 57, 2022–2040, https://doi.org/10.1175/1520-0469(2000)057<2022:CRMOTC>2.0.CO;2, 2000.

Held, I. M.: The Gap between Simulation and Understanding in Climate Modeling, Bull. Amer. Meteor. Soc., 86, 1609–1614, https://doi.org/10.1175/bams-86-11-1609, 2005.

Held, I. M., Hemler, R. S., and Ramaswamy, V.: Radiative-convective equilibrium with explicit two-dimensional moist convection, J. Atmos. Sci, 50, 3909–3927, 1993.

Held, I. M., Zhao, M., and Wyman, B.: Dynamic radiative-convective equilibria using GCM column physics, J. Atmos. Sci., 64, 228–238, https://doi.org/10.1175/JAS3825.11, 2007.

Hohenegger, C., Korn, P., Linardakis, L., Redler, R., Schnur, R., Adamidis, P., Bao, J., Bastin, S., Behravesh, M., Bergemann, M., Biercamp, J., Bockelmann, H., Brokopf, R., Brüggemann, N., Casaroli, L., Chegini, F., Datseris, G., Esch, M., George, G., Giorgetta, M., Gutjahr, O., Haak, H., Hanke, M., Ilyina, T., Jahns, T., Jungclaus, J., Kern, M., Klocke, D., Kluft, L., Kölling, T., Kornblueh, L., Kosukhin, S., Kroll, C., Lee, J., Mauritsen, T., Mehlmann, C., Mieslinger, T., Naumann, A. K., Paccini, L., Peinado, A., Praturi, D. S., Putrasahan, D., Rast, S., Riddick, T., Roeber, N., Schmidt, H., Schulzweida, U., Schütte, F., Segura, H., Shevchenko, R., Singh, V., Specht, M., Stephan, C. C., von Storch, J.-S., Vogel, R., Wengel, C., Winkler, M., Ziemen, F., Marotzke, J., and Stevens, B.: ICON-Sapphire: simulating the components of the Earth system and their interactions at kilometer and subkilometer scales, Geosci. Model Dev., 16, 779–811, https://doi.org/10.5194/gmd-16-779-2023, 2023.

https://doi.org/10.5194/gmd-2023-235
Preprint. Discussion started: 18 December 2023

Hourdin, F. and coauthors: LMDZ6A: The atmospheric component of the ISPL climate model with improved and better tuned physics, J. Adv. Model. Earth Syst., 12, e2019MS001 892, https://doi.org/10.1029/2019MS001892, 2020.

Jeevanjee, N., Hassanzadeh, P., Hill, S. A., and Sheshadri, A.: A perspective on climate model hierarchies, J. Adv. Model. Earth Sys., https://doi.org/10.1002/2017MS001038, 2017.

Khairoutdinov, M. F. and Emanuel, K.: Rotating radiative-convective equilibrium simulated by a cloud-resolving model, J. Adv. Model. Earth Sys., 5, https://doi.org/10.1002/2013MS000253, 2013.

Khairoutdinov, M. F. and Randall, D.: Cloud resolving modeling of the ARM Summer 1997 IOP: Model formulation, results, uncertainties, and sensitivities, J. Atmos. Sci., 60, 607–625, 2003.

Khairoutdinov, M. F., Blossey, P. N., and Bretherton, C. S.: Global System for Atmospheric Modeling: Model Description and Preliminary Results, J. Adv. Model. Earth Sys., 14, e2021MS002 968, https://doi.org/https://doi.org/10.1029/2021MS002968, 2022.

Klein, S. A. and Jakob, C.: Validation and senstiivities of frontal clouds simulated by the ECMWF model, Mon. Wea. Rev., 127, 2514–2531, 1999.

Lac, C., Chaboureau, J.-P., Masson, V., Pinty, J.-P., Tulet, P., Escobar, J., Leriche, M., Barthe, C., Aouizerats, B., Augros, C., Aumond, P., Auguste, F., Bechtold, P., Berthet, S., Bielli, S., Bosseur, F., Caumont, O., Cohard, J.-M., Colin, J., Couvreux, F., Cuxart, J., Delautier, G., Dauhut, T., Ducrocq, V., Filippi, J.-B., Gazen, D., Geoffroy, O., Gheusi, F., Honnert, R., Lafore, J.-P., Lebeaupin Brossier, C., Libois, Q., Lunet, T., Mari, C., Maric, T., Mascart, P., Mogé, M., Molinié, G., Nuissier, O., Pantillon, F., Peyrillé, P., Pergaud, J., Perraud, E., Pianezze, J., Redelsperger, J.-L., Ricard, D., Richard, E., Riette, S., Rodier, Q., Schoetter, R., Seyfried, L., Stein, J., Suhre, K., Taufour, M., Thouron, O., Turner, S., Verrelle, A., Vié, B., Visentin, F., Vionnet, V., and Wautelet, P.: Overview of the Meso-NH model version 5.4 and its applications, Geosci. Model Dev., 11, 1929–1969, https://doi.org/10.5194/gmd-11-1929-2018, 2018.

Lindzen, R. S. and Nigam, S.: On the role of sea surface temperature gradients in forcing low-level winds and convergence in the tropics, J. Atmos. Sci., 44, 2418–2436, 1987.

Liu, C. and Moncrieff, M. W.: Explicitly simulated tropical convection over idealized warm pools, J. Geophys. Res., 113, D21 121, https://doi.org/10.1029/2008JD010206, 2008.

Lutsko, N. and Cronin, T.: Mean climate and circulation of mock-Walker simulations, J. Adv. Model. Earth Syst., p. in review, 2022.

Lutsko, N. J. and Cronin, T. W.: Increase in precipitation efficiency with surface warming in radiative-convective equilibrium, J. Adv. Model. Earth Syst., 10, 2992–3010, https://doi.org/10.1029/2018MS001482, 2018.

Manabe, S. and Strickler, R. F.: Thermal equilibriation of the atmosphere with a convective adjustment, J. Atmos. Sci., 21, 361–385, 1964.

Morrison, H. and Milbrandt, J. A.: Parameterization of cloud microphysics based on the prediction of bulk ice particle properties. Part I: Scheme description and idealized tests, J. Atmos. Sci., 72, 287–311, 2015.

Morrison, H., Curry, J., and Khvorostyanov, V.: A new double-moment microphysics parameterization for application in cloud and climate models. Part I: Description, J. Atmos. Sci., 62, 1665–1677, 2005.

Müller, S. K. M. and Hohenegger, C.: Self-aggregation of convection in spatially-varying sea surface temperatures, J. Adv. Model. Earth Syst., 12, e2019MS001 698, https://doi.org/10.1029/2019MS001698., 2020.

Neale, R., Chen, C.-C., Gettelman, A., Lauritzen, P., Park, S., WIlliamson, D., Conley, A., Garcia, R., Kinnison, D., Lamarque, J.-F., Marsh, D., Mills, M., Smith, A., Tilmes, S., Vitt, F., Morrison, H., Cameron-Smith, P., Collins, W., Iacono, M., Easter, R., Ghan, S., Liu, X., Rasch, P., and Taylor, M.: Description of the NCAR Community Atmosphere Model (CAM 5.0), NCAR Tech. Note TN-486, http://www.cesm.ucar.edu/models/cesm1.0/cam/docs/description/cam5_desc.pdf, 2012.

https://doi.org/10.5194/gmd-2023-235
Preprint. Discussion started: 18 December 2023

Nishizawa, S., Yashiro, H., Sato, Y., Miyamoto, Y., and Tomita, H.: Influence of grid aspect ratio on planetary boundary layer turbulence in large-eddy simulations, Geosci. Model Dev., 8, 3393–3419, https://doi.org/10.5194/gmd-8-3393-2015, 2015.

Pope, K. N., Holloway, C. E., Jones, T. R., and Stein, T. H. M.: Radiation, Clouds, and Self-Aggregation in RCEMIP Simulations, J. Adv. Model. Earth Sys., 15, e2022MS003 317, https://doi.org/https://doi.org/10.1029/2022MS003317, 2023.

Popke, D., Stevens, B., and Voigt, A.: Climate and climate change in a radiative-convective equilibrium version of ECHAM6, J. Adv. Model. Earth Sys., 5, 1–14, https://doi.org/10.1029/2012MS000191, 2013.

Randall, D. A., DeMott, C., Stan, C., Khairoutdinov, M., Benedict, J., McCrary, R., Thayer-Calder, K., and Branson, M.: Simulations of the Tropical General Circulation with a Multiscale Global Model, Meteorological Monographs, 56, 15.1–15.15, https://doi.org/10.1175/amsmonographs-d-15-0016.1, 2016.

Raymond, D. J.: Convective processes and tropical atmospheric circulations, Q. J. Roy. Meteor. Soc., 120, 1431–1455, https://doi.org/10.1002/qj.49712052002, 1994.

Rayner, N. A., Parker, D. E., Horton, E. B., Folland, C. K., Alexander, L. V., Powell, D. P., Kent, E. C., and Kaplan, A.: Global analyses of sea surface temperature, sea ice, and night marine air temperature since the late nineteenth century, J. Geophys. Res., 108, 4407, https://doi.org/https://doi.org/10.1029/2002JD002670, 2023.

Reed, K. A., Silvers, L. G., Wing, A. A., Hu, I.-K., and Medeiros, B.: Using Radiative Convective Equilibrium to Explore Clouds and Climate in the Community Atmosphere Model, J. Adv. Model. Earth Sys., 13, e2021MS002 539, https://doi.org/https://doi.org/10.1029/2021MS002539, 2021.

Roehrig, R. and coauthors: The CNRM global atmosphere model ARPEGE-Climate 6.3: description and evaluation, J. Adv. Model. Earth Syst., 12, e2020MS002 075, https://doi.org/10.1029/2020MS002075, 2020.

Romps, D. M.: The dry-entropy budget of a moist atmosphere, J. Atmos. Sci., 65, 3779–3799, 2008.

Sato, Y., Nishizawa, S., Yashiro, H., Miyamoto, Y., Kajikawa, Y., and Tomita, H.: Impacts of cloud microphysics on trade wind cumulus: which cloud microphysics processes contribute to the diversity in a large eddy simulation?, Prog. Earth Planet. Sci., 2, 23, https://doi.org/10.1186/s40645-015-0053-6, 2015.

Satoh, M., Tomita, H., Yashiro, H., Miura, H., Kodama, C., Seiki, T., Noda, A. T., Yamada, Y., Goto, D., Sawada, M., Miyoshi, T., Niwa, Y., Hara, M., Ohno, T., Iga, S.-I., Inoue, T. A. T., and Kubokawa, H.: The Non-hydrostatic ICosahedral Atmospheric Model: Description and development, Progress in Earth and Planetary Science, 1, 18, https://doi.org/10.1186/s40645-014-0018-1, 2014.

Satoh, M., Arakami, K., and Sawada, M.: Structure of tropical convective systems in aqua-planet experiments: Radiative-convective equilibrium versus the Earth-like experiments, SOLA, 12, 220–224, 2016.

Silvers, L., Reed, K., and Wing, A.: The Response of the Large-Scale Tropical Circulation to Warming, J. Adv. Model. Earth Syst., 15, https://doi.org/10.1029/2021MS002966, 2023.

Silvers, L. G. and Robinson, T.: Clouds and radiation in a Mock-Walker circulation, J. Adv. Model. Earth Syst., 13, e2020MS002 196, https://doi.org/10.1029/2020MS002196, 2021.

Stauffer, C. and Wing, A.: Properties, changes, and controls of deep-convecting clouds in Radiative-Convective Equilibrium, J. Adv. Model. Earth Syst., 14, e2021MS002 917, https://doi.org/10.1029/2021MS002917, 2022.

Stauffer, C. L.: Cloud Feedbacks and Convective Self-Aggregation in the Radiative-Convective Equilibrium Model Intercomparison Project, Ph.D. thesis, Florida State University, Tallahassee, FL, https://fsu-flvc.primo.exlibrisgroup.com/permalink/01FALSC_FSU/1pc67ru/cdi_proquest_journals_2868559250, 219 pp., 2023.

https://doi.org/10.5194/gmd-2023-235
Preprint. Discussion started: 18 December 2023

Stauffer, C. L. and Wing, A. A.: Explicitly Resolved Cloud Feedbacks in the Radiative-Convective Equilibrium Model Intercomparison Project, J. Adv. Model. Earth Sys., 15, e2023MS003 738, https://doi.org/https://doi.org/10.1029/2023MS003738, 2023a.

Stauffer, C. L. and Wing, A. A.: How Does Organized Convection Impact Explicitly Resolved Cloud Feedbacks in the Radiative-Convective Equilibrium Model Intercomparison Project,, J. Adv. Model. Earth Sys., p. in review, 2023b.

Stratton, R., Senior, C., Vosper, S., Folwell, S., Boutle, I., Earnshaw, P., Kendon, E., Lock, A., Malcolm, A., Manners, J., Morcrette, C., Short, C., Stirling, A. J., Taylor, C. M., Tucker, S., Webster, S., and Wilkinson, J. M.: A Pan-African convection-permitting regional climate simulation with the Met Office Unified Model: CP4-Africa, J. Climate, 31, 3485–3508, 2018.

Tompkins, A. M.: On the relationship between tropical convection and sea surface temperature, J. Climate, 14, 633–637, https://doi.org/10.1175/1520-0442(2001)014<0633:OTRBTC>2.0.CO;2, 2001.

Tompkins, A. M. and Craig, G. C.: Radiative-convective equilibrium in a three-dimensional cloud-ensemble model, Q. J. R. Meteorol. Soc., 124, 2073–2097, 1998.

Voldoire, A., Saint-Martin, D., Sénési., S., Decharme, B., Alias, A., Chevallier, M., Colin, J., Guérémy, J.-F., Michou, M., Moine, M.-P., Nabat, P., Roehrig, R., y Mélia, D. S., Séférian, R., Valcke, S., Beau, I., Belamari, S., Berthet, S., Cassou, C., Cattiaux, J., Deshayes, J., Douville, H., Ethé, C., Franchistéguy, L., Geoffroy, O., Lévy, C., Madec, G., Meurdesoif, Y., Msadek, R., Ribes, A., Sanchez-Gomez, E., Terray, L., and Waldman, R.: Evaluation of CMIP6 DECK expeirments with CNRM-CM6.1., J. Adv. Model. Earth Syst., 11, 2177–2213, https://doi.org/10.1029/2019MS001683, 2019.

Walters, D., Baran, A. J., Boutle, I., Brooks, M., Earnshaw, P., Edwards, J., Furtado, K., Hill, P., Lock, A., Manners, J., Morcrette, C., Mulcahy, J., Sanchez, C., Smith, C., Stratton, R., Tennant, W., Tomassini, L., Van Weverberg, K., Vosper, S., Willett, M., Browse, J., Bushell, A., Carslaw, K., Dalvi, M., Essery, R., Gedney, N., Hardiman, S., Johnson, B., Johnson, C., Jones, A., Jones, C., Mann, G., Milton, S., Rumbold, H., Sellar, A., Ujiie, M., Whitall, M., Williams, K., and Zerroukat, M.: The Met Office Unified Model Global Atmosphere 7.0/7.1 and JULES Global Land 7.0 configurations, Geoscientific Model Development, 12, 1909–1963, https://doi.org/10.5194/gmd-12-1909-2019, 2019.

Webb, M., Senior, C., Bony, S., and Morcrette, J. J.: Combining ERBE and ISCCP data to assess clouds in the Hadley Centre, ECWMF and LMD atmospheric climate models, Climate Dyn., 17, 905–922, 2001.

Wing, A. A. and Silvers, L.: Code and data for RCEMIP-II: Mock-Walker Simulations as Phase II of the Radiative-Convective Equilibrium Model Intercomparison Project (v1.0), https://doi.org/10.5281/zenodo.10137266, 2023.

Wing, A. A. and Singh, M. S.: Control of Stability and Relative Humidity in the Radiative-Convective Equilibrium Model Intercomparison Project, J. Adv. Model. Earth Sys., p. accepted, 2023.

Wing, A. A., Reed, K. A., Satoh, M., Stevens, B., Bony, S., and Ohno, T.: Radiative-Convective Equilibrium Model Intercomparison Project, Geosci. Model Dev., 11, 793–813, https://doi.org/10.5194/gmd-11-793-2018, 2018.

Wing, A. A., Stauffer, C., Becker, T., Reed, K., Ahn, M.-S., Arnold, N., Bony, S., Branson, M., Bryan, G., Chaboureau, J.-P., de Roode, S., Gayatri, K., Hohenegger, C., Hu, I.-K., Jansson, F., Jones, T., Khairoutdionv, M., Kim, D., Martin, Z., Matsugishi, S., Medeiros, B., Miura, H., Moon, Y., Möller, S., Ohno, T., Popp, M., Prabhakaran, T., Randall, D., Rios-Berrios, R., Rochetin, N., Roehrig, R., Romps, D., Jr., J. R., Satoh, M., Silvers, L., Singh, M., Stevens, B., Tomassini, L., van Heerwaarden, C., Wang, S., and Zhao, M.: Clouds and convective self-aggregation in a multi-model ensemble of radiative-convective equilibrium simulations, J. Adv. Model. Earth Syst., 12, e2020MS002 138, https://doi.org/10.1029/2020MS002138, 2020a.

Wing, A. A., Stauffer, C., Becker, T., Reed, K., Ahn, M.-S., Arnold, N., Bony, S., Branson, M., Bryan, G., Chaboureau, J.-P., de Roode, S., Gayatri, K., Hohenegger, C., Hu, I.-K., Jansson, F., Jones, T., Khairoutdionv, M., Kim, D., Martin, Z., Matsugishi, S., Medeiros,

https://doi.org/10.5194/gmd-2023-235
Preprint. Discussion started: 18 December 2023

B., Miura, H., Moon, Y., Möller, S., Ohno, T., Popp, M., Prabhakaran, T., Randall, D., Rios-Berrios, R., Rochetin, N., Roehrig, R., Romps, D., Jr., J. R., Satoh, M., Silvers, L., Singh, M., Stevens, B., Tomassini, L., van Heerwaarden, C., Wang, S., and Zhao, M.: Radiative-Convective Equilibrium Model Intercomparison Project (RCEMIP) Simulation Dataset, http://hdl.handle.net/21.14101/d4beee8e-6996-453e-bbd1-ff53b6874c0e, 2020b.

Wofsy, J. and Kuang, Z.: Cloud-resolving model simulations and a simple model of an idealized Walker cell, J. Climate, 25, 8090–8107, https://doi.org/10.1175/JCLI-D-11-00692.1, 2012.

Wu, C.-M., Lin, H.-C., Cheng, F.-Y., and Chien, M.-H.: Implementation of the Land Surface Processes into a Vector Vorticity Equation Model (VVM) to Study its Impact on Afternoon Thunderstorms over Complex Topography in Taiwan, Asia-Pacific Journal of Atmospheric Sciences, 55, 701–717, https://doi.org/10.1007/s13143-019-00116-x, 2019.

Zelinka, M. D., Klein, S. A., and Hartmann, D. L.: Computing and partitioning cloud feedbacks using cloud property histograms. Part I: Cloud radiative kernels, J. Climate, 25, 3715–3735, https://doi.org/10.1175/JCLI-D-11-00248.1, 2012a.

Zelinka, M. D., Klein, S. A., and Hartmann, D. L.: Computing and partitioning cloud feedbacks using cloud property hitsograms. Part II: Attribution to changes in cloud amount, altitude, and optical depth, J. Climate, 25, 3736–3754, https://doi.org/10.1175/JCLI-D-11-00249.1, 2012b.

Zelinka, M. D., Klein, S. A., Taylor, K. E., Andrews, T., Webb, M. J., Gregory, J. M., and Forster, P. M.: Contributions of different cloud types to feedbacks and rapid adjustments in CMIP5, J. Climate, 26, 5007–5027, https://doi.org/10.1175/JCLI-D-12-00555.1, 2013.

Zhao, M., Golaz, J.-C., Held, I. M., Guo, H., Balaji, V., Benson, R., Chen, J.-H., Chen, X., Donner, L. J., Dunne, J. P., Dunne, K., Durachta, J., Fan, S.-M., Freidenreich, S. M., Garner, S. T., Ginoux, P., Harris, L. M., Horowitz, L. W., Krasting, J. P., Langenhorst, A. R., Liang, Z., Lin, P., Lin, S.-J., Malyshev, S. L., Mason, E., Milly, P. C. D., Ming, Y., Naik, V., Paulot, F., Paynter, D., Philipps, P., Radhakrishnan, A., Ramaswamy, V., Robinson, T., Schwarzkopf, D., Seman, C. J., Shevliakova, E., Shen, Z., Shin, H., Silvers, L. G., Wilson, J. R., Winton, M., Wittenberg, A. T., Wyman, B., and Xiang, B.: The GFDL global atmosphere and land model AM4.0/LM4.0: 1. Simulation characteristics with prescribed SSTs, J. Adv. Model. Earth Syst., 10, 691–734, https://doi.org/10.1002/2017MS001208, 2018a.

Zhao, M., Golaz, J.-C., Held, I. M., Guo, H., Balaji, V., Benson, R., Chen, J.-H., Chen, X., Donner, L. J., Dunne, J. P., Dunne, K., Durachta, J., Fan, S.-M., Freidenreich, S. M., Garner, S. T., Ginoux, P., Harris, L. M., Horowitz, L. W., Krasting, J. P., Langenhorst, A. R., Liang, Z., Lin, P., Lin, S.-J., Malyshev, S. L., Mason, E., Milly, P. C. D., Ming, Y., Naik, V., Paulot, F., Paynter, D., Philipps, P., Radhakrishnan, A., Ramaswamy, V., Robinson, T., Schwarzkopf, D., Seman, C. J., Shevliakova, E., Shen, Z., Shin, H., Silvers, L. G., Wilson, J. R., Winton, M., Wittenberg, A. T., Wyman, B., and Xiang, B.: The GFDL global atmosphere and land model AM4.0/LM4.0: 2. Model description, sensitivity studies, and tuning strategies, J. Adv. Model. Earth Syst., 10, 735–769, https://doi.org/10.1002/2017MS001209, 2018b.

Zhou, L., Lin, S.-J., Chen, J.-H., Harris, L. M., Chen, X., and Rees, S. L.: Toward Convective-Scale Prediction within the Next Generation Global Prediction System, Bull. Amer. Meteor. Soc., 100, 1225–1243, https://doi.org/10.1175/bams-d-17-0246.1, 2019.

Zhu, J., Otto-Bliesner, B. L., Brady, E. C., Gettelman, A., Bacmeister, J. T., Neale, R. B., Poulsen, C. J., Shaw, J. K., McGraw, Z. S., and Kay, J. E.: LGM Paleoclimate Constraints Inform Cloud Parameterizations and Equilibrium Climate Sensitivity in CESM2, J. Adv. Model. Earth Sys., 14, e2021MS002 776, https://doi.org/10.1029/2021MS002776, 2022.